RSC Sustainability

ROYAL SOCIETY OF CHEMISTRY

TUTORIAL REVIEW

View Article Online
View Journal | View Issue

Cite this: *RSC Sustainability*, 2023, **1**, 38

Sustainability applications of rare earths from metallurgy, magnetism, catalysis, luminescence to future electrochemical pseudocapacitance energy storage

Shan-Shan Chai,[a] Wei-Bin Zhang, *[a] Jing-Lei Yang,[a] Lun Zhang,[a] Myat Myintzu Theint,[b] Xian-Li Zhang,[a] Shao-Bo Guo,[a] Xia Zhou[a] and Xue-Jing Ma *[a]

Rare Earths (REs) are referred to as 'industrial vitamins' and play an indispensable role in a variety of domains. This article reviews the applications of REs in traditional metallurgy, biomedicine, magnetism, luminescence, catalysis, and energy storage, where it is surprising to discover the infinite potential of REs in electrochemical pseudocapacitive energy storage. The use of REs in the field of pseudocapacitance is an important opportunity to link resources with burgeoning electrochemical energy storage. On the basis of the electrochemical energy storage potential of REs, typical rare earth oxides are selected as research objects to provide a comprehensive overview of their research progress in the field of supercapacitors. The future challenges and opportunities that these compounds will encounter in the field of pseudocapacitance energy storage are evaluated with a summary and discussion of existing research outcomes.

Received 20th September 2022
Accepted 19th November 2022

DOI: 10.1039/d2su00054g

rsc.li/rscsus

Sustainability spotlight

Based on the current situation of increasing energy demand and environmental pollution, the development of new sustainable energy sources has become a key issue. In accordance with the UN SDG "Ensuring Access to Affordable, Reliable, and Sustainable Modern Energy for All", this paper investigates the unlimited potential of abundant and environmentally friendly rare-earth-based compounds for sustainable electrochemical storage applications. Rare earth compounds are ideal electrode materials due to their environmental friendliness, abundant supply, easy preparation, and excellent redox capacitance properties. This paper presents a comprehensive overview and future application prospects of rare earth compounds in the field of pseudocapacitance to provide readers with more effective preparation strategies and future development directions for pseudocapacitive electrode materials based on rare-earth-based compounds.

1 Introduction

Sustainability of the energy supply and resolving the problem of environmental pollution are challenging issues that must be resolved in today's and future societies.[1–3] In light of the current situation of rising energy demand and worsening environmental pollution, the development of new sustainable energy sources has emerged as a paramount concern in the energy sector.[4,5] Right now the ideal replacement for nonrenewable energy sources like fossil fuels is hydrogen energy because of its high calorific value (120 MJ kg^{-1}) and lack of pollutants.[6,7] However, present hydrogen storage technologies have inherent flaws, such as low efficiency and a propensity to leak.[8] It is critical to create innovative and effective energy storage technologies given the present issues with hydrogen energy storage and the intermittent release of energy from renewable energy sources.[9,10]

Current representative electrochemical energy storage devices include lithium-ion batteries and supercapacitors.[11] Lithium-ion batteries will not be able to meet future needs for more energy use, faster power transfer, and better cycle stability because they have a low power density and are unstable.[12] Supercapacitors make up for this lack and have been extensively studied.[13–15] Electrodes in supercapacitor energy storage devices determine electrochemical performance.[16] Consequently, the development of novel electrode materials is the next research priority.

Rare Earths (REs), commonly referred to as rare earth metals, comprise a total of 17 elements, including scandium (Sc), yttrium (Y), and lanthanides.[17] Due to their unique electronic structure, rare earth elements feature optical, electrical, magnetic, and catalytic capabilities not found in other

[a]College of Materials and Chemistry & Chemical Engineering, Chengdu University of Technology, Chengdu 610059, China. E-mail: zhangweibin17@cdut.edu.cn; maxuejing17@cdut.edu.cn

[b]Mineral Development Section for International Relation, Department of Mines, Ministry of Natural Resources and Environmental, Nay Pyi Taw 15011, Myanmar

elements; consequently, they are used in practically every industry.[18] Sc and Y, for instance, are essential components for improving the crystal structure and mechanical properties of steels and alloys.[19] Nd and Sm are the necessary raw materials for the manufacture of permanent magnets.[20] Ce and Eu are highly efficient luminous materials for activating ions due to their unusual 4f–5d electronic transitions, which allow them to emit light at all wavelengths.[21] In the sectors of air purification and ammonia production, the Ce-based catalyst has an indispensable position.[22] In recent years, REs have been extensively utilized in the energy storage industry. $LaNi_5$ is a solid-state hydrogen storage material of superior efficiency.[23] REs affect the cathode materials of lithium-ion batteries (such as $LiCoO_2$ and $LiMn_2O_4$) to distort the lattice, hence enhancing the conductivity of the electrode material, and restricting the dissolution of Mn to enhance the electrode material's electrochemical performance.[24,25] Some researchers have uncovered the inexhaustible potential of rare earths in the realm of pseudocapacitive energy storage through wide application and in-depth investigation.[26,27] In prior research, rare earth elements were frequently considered electrochemically inert. Therefore, the abundant rare earth resources have been neglected in the field of pseudocapacitors. However, the majority of rare earth elements show RE^{3+}/RE^{2+} or RE^{4+}/RE^{3+} redox coupling, laying the thermodynamic groundwork for their employment in pseudocapacitive energy storage.[28] In addition, the aforementioned redox couples are active in organic solvents and aqueous environments and can be utilized as redox-active components in pseudocapacitive energy storage.

In this review, we introduce the applications of rare earths in traditional metallurgy, biomedicine, magnetism, luminescence, catalysis, and energy storage. The research advances of typical oxides in rare earth compounds in the field of pseudocapacitors is highlighted, including the energy storage mechanism and electrochemical performance. In addition, future challenges and opportunities for rare earth compounds in the realm of pseudocapacitive energy storage are elaborated upon.

2 Elementary rare earths

2.1 Elementary rare earth elements

Rare earth elements (REs), also known as rare earth metals, are made up of 17 different elements, including scandium (Sc), yttrium (Y), and lanthanide elements from the third subgroup.[29] According to the regulations of the International Union of Pure and Applied Chemistry (IUPAC), the elements with atomic numbers 57–71 (blue in Fig. 1): lanthanum (La), cerium (Ce), praseodymium (Pr), neodymium (Nd), promethium (Pm), samarium (Sm), europium (Eu), gadolinium (Gd), terbium (Tb), dysprosium (Dy), holmium (Ho), erbium (Er), thulium (Tm), ytterbium (Yb), and lutetium (Lu), are called the lanthanide elements.[30] When the electrons of lanthanide atoms occupy the 4f orbital of the inner layer, an electron in the same 4f orbital cannot be completely shielded by another electron.[31] Consequently, when the atomic number increases, the number of effective nuclear charges acting on each 4f electron increases, resulting in a decrease in radius; this phenomenon is known as

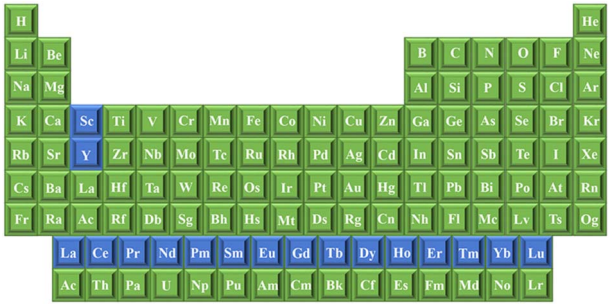

Fig. 1 Periodic table of the elements, with the rare earths shown in blue.

'lanthanide shrinkage'. Table 1 displays the atomic mass, outer electron, spectral ground state, and other characteristics of rare earth elements.[29–31] 16 of the 17 rare earth elements, except scandium (Sc), are separated into two categories based on the electronic layer structure and the physical and chemical properties of the reaction: light rare earths and heavy rare earths. La, Ce, Pr, Nd, Pm, Sm, and Eu are cerium-group rare earths, that is, light rare earths (L-RE); Gd, Tb, Dy, Ho, Er, Tm, Yb, Lu, and Y are yttrium-group rare earths, that is, heavy rare earths (H-RE).

The earth's crust contains up to 153 g t^{-1} of rare earth elements, the most abundant of which is cerium. The distribution of rare earth elements conforms to the Oddo–Harkins rule, which states that elements with even atomic numbers are more abundant than nearby elements with odd atomic numbers. Rare earth elements exist in three distinct forms: I. those that participate in lattice and rare earth symbiosis to form minerals containing rare earth elements, such as monazite and bastnasite; II. those that undergo isomorphic substitution, Ca, Sr, Ba, Mn, Zr, *etc.*, are scattered throughout minerals such as apatite, europium titanite, *etc.*; III. those whose ions are adsorbed on the surface of minerals or between grains, including clay minerals, mica ore, *etc.* In minerals, rare earth elements are mostly found as ionic compounds, which make up the coordination polyhedrons.

2.2 Typical applications fields

Due to their distinctive electronic structure, rare earth elements possess optical, electrical, and magnetic capabilities not seen in other elements.[32] As 'contemporary industrial vitamins', rare earths and their derivatives are widely utilized in traditional materials and emerging industries.[33]

2.2.1 Traditional fields. The application of rare earth elements in metallurgy, such as enhancing the characteristics of steel and alloys, is the most significant field in traditional industrial applications.[34] Heterogeneous nucleation in steel controls the crystallization, segregation, grain development, and phase transformation processes throughout metallurgical processes.[35,36] Numerous investigations have proven the tight relationship between heterogeneous nucleation and the type of oxidant utilized in the metallurgical process: the grain size of austenite, the oxygen concentration, the rate of cooling, and the nucleation temperature.[37,38] Adding rare earth metals to steel is

Table 1 Atomic mass, outer electron, and spectral ground state of the rare earth elements[29–31]

Element	Atomic number	Relative atomic mass	Electronic configuration of atoms	Electronic configuration of RE^{2+}	Electronic configuration of RE^{3+}	Spectral ground state notation	Electronic configuration of RE^{4+}
Sc	21	44.95591	$3d^14s^2$	—	—	—	—
Y	39	88.90585	$4d^15s^2$	—	—	—	—
La	57	138.9055	$5d^16s^2$	$5d^1$	—	—	—
Ce	58	140.115	$4f^26s^2$	$4f^2$	$4f^1$	$^2F_{5/2}$	$5s^25p^6$
Pr	59	140.90765	$4f^36s^2$	$4f^3$	$4f^2$	$^3H_4$	$4f^15s^65p^6$
Nd	60	144.24	$4f^46s^2$	$4f^4$	$4f^3$	$^4I_{9/2}$	$4f^25s^25p^6$
Pm	61	145	$4f^56s^2$	$4f^5$	$4f^4$	$^5I_4$	
Sm	62	150.36	$4f^66s^2$	$4f^6$	$4f^5$	$^6H_{5/2}$	—
Eu	63	151.965	$4f^76s^2$	$4f^7$	$4f^6$	$^7F_0$	—
Gd	64	157.25	$4f^75d^16s^2$	$4f^8$	$4f^7$	$^8S_{7/2}$	—
Tb	65	158.92534	$4f^96s^2$	$4f^9$	$4f^8$	$^7F_6$	$4f^75s^25p^6$
Dy	66	162.50	$4f^{10}6s^2$	$4f^{10}$	$4f^9$	$^6H_{15/2}$	$4f^85s^25p^6$
Ho	67	164.93032	$4f^{11}6s^2$	$4f^{11}$	$4f^{10}$	$^5I_8$	—
Er	68	167.26	$4f^{12}6s^2$	$4f^{12}$	$4f^{11}$	$^4I_{15/2}$	—
Tm	69	168.93421	$4f^{13}6s^2$	$4f^{13}$	$4f^{12}$	$^3H_6$	—
Yb	70	173.04	$4f^{14}6s^2$	$4f^{14}$	$4f^{13}$	$^2F_{7/2}$	—
Lu	71	174.967	$4f^{14}5d^16s^2$	—	$4f^{14}$	—	—

one of the most effective methods to address the aforementioned problems and improve the overall performance of steel. Rare earth elements readily lose electrons and transform into positive ions.[39] Rare earth metals with extraordinarily high chemical activity react with sulfur and oxygen to entirely deoxidize and desulfurize steel, limiting the negative influence of impurities on its qualities and boosting its mechanical properties.[40] In addition, the presence of rare earth elements in steel can alter the distribution of impurities and refine the rigid body structure. As a result, the rigid body microstructure distribution is more uniform, exhibiting greater microhardness, and the corrosion resistance of steel is significantly enhanced.[41]

The vast majority of research on rare earth alloys focuses on lightweight magnesium (Mg) alloys, which are widely employed in high-performance automobiles and the aerospace industry.[42] Mg-based alloys are suited for application in gravity-sensitive devices due to Mg's low density of 1.7 g cm^{-3}, which is the lowest among typical structural metals. However, their poor ductility and susceptibility to corrosion in liquid environments restrict their widespread utilization.[43] Adjusting the metallurgical conditions can successfully improve the plasticity issue, whereas the corrosion issue continues to be the primary focus and challenge of current research in the field of Mg-alloys. The large negative free energy on the surface of Mg-alloys might facilitate the rapid formation of an oxidation/hydroxide layer, but the oxidation/hydroxide layer cannot prevent corrosion due to the following issues: I. the majority of the oxidation/hydroxide film is soluble in water. II. The oxidation/hydroxide film cannot completely cover the alloy. III. Galvanic corrosion cannot be avoided in magnesium alloys with high negative potential.[44–46]

Doping with rare earth elements presents a potential solution to the problems outlined.[47] The effect of doping with rare earth elements is clarified below, using magnesium-based alloys as an illustration. In 2003, Morales *et al.* investigated the corrosion behavior of magnesium alloys containing rare earth metals in NaCl solution.[48] Studies indicate that rare earth elements can effectively block the hydrogen evolution process in corrosion and significantly enhance the corrosion resistance of magnesium alloys. Hort *et al.* also confirmed the influence of rare earth elements on the improvement of magnesium alloys' corrosion resistance.[49] Notably, only when the rare earth element Gd occurs as a solid solution in the magnesium alloy is its performance significantly enhanced. When the precipitation phase appears, in contrast, it promotes the occurrence of corrosion. Consequently, Schlüter and his team fabricated MgY and MgGd alloy thin films by sputter deposition.[50] The film is not only resistant to corrosion but also exhibits remarkable mechanical properties. Due to the fact that the atomic radius and electronegativity of rare earth elements are comparable to those of magnesium, it is simple for them to create solid solutions with magnesium alloys. The rare earth oxides and sulfides produced by eliminating O, S, and other impurities from magnesium alloys have a minor potential difference with the magnesium matrix, thereby preventing corrosion. Doping with rare earths can effectively inhibit the formation of precipitates and produce solid-solution strengthening. Therefore, doping with rare earth elements can not only effectively improve the corrosion resistance of magnesium alloys but also change the texture of the alloy, refine the grains, and improve its mechanical properties.[51,52] This opens up a new vista for the improvement of established metallurgical procedures in order to produce high-performance magnesium alloys. Based on the corrosion resistance and excellent mechanical properties of the RE-Mg alloys mentioned above, RE-Mg alloys show great application potential as degradable alloys in the field of biomedicine.[53] Except for Pm, which is radioactive, the remaining rare earth elements have excellent biocompatibility at low doses. Numerous studies have determined that the rare earth elements (Y, Nd, Gd, Dy, Ho, *etc.*) have no effect on cellular

metabolism, although La and Ce should be added with caution to avoid adverse reactions, such as gas embolism and tissue necrosis. Table 2 is a summary of the research that has been done on rare earth Mg-alloys used in medicine.[54–61]

In general, the addition of rare earths to magnesium alloys not only provides advantages in reducing pollution, alleviating corrosion, and improving mechanical properties, but also plays an important role in the application of alloys in the circular economy in terms of low cost and efficient recycling. Current market developments indicate that the use of La and Ce instead of Mg in future alloy design concepts has incomparable advantages in terms of reducing environmental pollution and improving cost-effectiveness.

2.2.2 Rare earth magnetic materials. Rare-earth-based materials derive their magnetic characteristics mostly from the partially empty 4f shell electrons of rare earth ions, which depends on the total orbital angular momentum L, the total spin angular momentum S, and the total angular momentum J. The magnetic moment (μ) can be calculated with eqn (1):[62]

$$\mu = g\sqrt{J(J+1)}(\text{B.M.}) \quad (1)$$

The value of the Lande factor, denoted by g, is:

$$g = 1 + \frac{J(J+1) + S(S+1) - L(L+1)}{2J(J+1)} \quad (2)$$

The value of the Bohr magneton B.M. is:

$$\text{B.M.} = \frac{eh}{4\pi mc} \quad (3)$$

where h is Planck's constant, e is the electron charge, m is the mass, and c is the speed of light.

There are as many as seven unpaired electrons in the 4f configuration of rare earth elements.[63] The orbital motion, spin motion, and spin–orbit coupling of these 4f electrons distinguish them from transition metals in their magnetism. Rare earth elements are the best option for permanent magnet materials and magnetic refrigeration materials due to their great paramagnetic susceptibility, saturation magnetization, magnetic anisotropy and magnetocaloric effect.[64–66] A permanent magnet material is a material that converts mechanical energy to electrical energy *via* a magnetic field, and it is a typical material for achieving high-efficiency and lightweight energy conversion.[67] They have widespread use in refrigerators, air conditioners, wind turbines, and other small electrical appliances and electric equipment.[68] Nd and Sm are the rare earth elements utilized most typically in permanent magnets.[69] Due to the extraordinary magnetic anisotropy and high energy product, nanostructured $SmCo_5$ and $Nd_2Fe_{14}B$ have become the key research objects among the numerous Nd-based and Sm-based compounds.[70] For the transition from rare earth resources to clean energy, $SmCo_5$ and $Nd_2Fe_{14}B$ are essential application materials, fully aligning with the Sustainable Development Goal (SDG): ensuring access to affordable, reliable, and sustainable modern energy for all. It has been discovered that the microstructures of $SmCo_5$ and $Nd_2Fe_{14}B$, such as particle size, shape, and interface, determine the coercivity and maximum energy product.[71] The most effective way of optimizing the magnetic characteristics of $SmCo_5$ and $Nd_2Fe_{14}B$ is, therefore, exact control over the microstructure. The control structure focuses mostly on the following three actions: I. regulating the grain size of the oxidation precursor; II. regulating the reduction–diffusion process of the oxidation precursor; and III. regulating the oxidation precursor's thermal stability, getting rid of reaction byproducts.[72] The majority of studies are centered on grain refining, grain boundary phase change, and grain boundary diffusion processes based on the preceding notions. Hou *et al.* pioneered the manufacture of $SmCo_5$ by annealing core/shell-structured Co/Sm_2O_3 nanoparticles at high temperatures, utilizing KCl as a dispersion medium to enhance the reduction of Sm_2O_3, prevent $SmCo_5$ from developing into single crystals, and address the question of refining grain size.[73] The synthesized $SmCo_5$ demonstrates a Curie temperature (T_c) of 1020 K, and a coercivity of up to 24 kOe at 100 K. Ma *et al.* proposed a novel strategy for precisely controlling the precursor size in order to produce highly magnetically anisotropic $SmCo_5$, employing a hydrothermal process to synthesize precursors consisting of sheet-like $Co(OH)_2$ (250–400 nm) and rod-like $Sm(OH)_3$ (15–20 nm), which were subsequently reduced to $SmCo_5$ nanosheets.[74] $SmCo_5$ nanosheets show substantial magnetic anisotropy and

Table 2 Research on rare earth Mg-alloys utilized in biomedicine[54–61]

REEs	Alloys	Research object	Biocompatibility	Application	Ref.
Y, Sc	Mg-3Sc-3Y	Mouse osteoblast cells	No cytotoxicity	Degradable implant material	54
Y, Nd	Mg-Nd-Y-Zr-Ca	Subcutaneous rat tissue	No toxicological or pathophysiological risks	Degradable implant material	55
Y, Nd	Mg–Zn–Y–Nd–Zr	L929 and MC3T3-E1 cells	Minimal cytotoxicity	Orthopaedic implant material	56
Y, Nd, Ce	Mg-RE	Vascular smooth muscle cells	Little effect on biological activity of vascular cells at low dose	Cardiovascular stent	57
Nd, Gd, Dy	Mg–Y–Zr–RE	Aortic endothelial cells	No deleterious effect on platelets and reduces platelet adhesion and activation	Vascular stent	58
Gd	Mg–Gd	Rat tissues	Accumulate in animal organs	Use with caution	59
Gd, Dy	WE43	RAW 264.7, MG63 and HUCPV cells	No cytotoxicity	High solid solution element	60
Nd, Pr, Eu			No cytotoxicity	Low solid solution element	
Ce, La			Influences viability of cells	Use with caution	
Ho	Mg–Zr–Sr–Ho	$SaOS_2$ cells	Little effect on cells at low dose	Orthopedic degradable material	61

excellent magnetic characteristics at room temperature. The coercivity of the $SmCo_5$ nanosheets was 19.3 kOe, and the maximal energy product reached 14.4 MGOe, which is the best performance among the $SmCo_5$ nanosheets yet synthesized. $Nd_2Fe_{14}B$ is prepared in a manner similar to $SmCo_5$, in which oxide precursors are reduced and transformed.[75] Notably, the saturated vapor pressure of Nd is higher than that of Sm, necessitating the addition of additional Nd_2O_3 to the precursor to compensate for the loss of Nd element during the evaporation process.[76] Current research findings on $Nd_2Fe_{14}B$-based permanent magnet materials are presented in Table 3, demonstrating that the selection of appropriate dispersants can effectively alter the kinetics of the reduction–diffusion reaction and optimize the crystal size of $Nd_2Fe_{14}B$.[77–80] Current research reveals that coupled $Nd_2Fe_{14}B$/α-Fe nanocomposites created by the reduction–diffusion process have higher coercivity than $Nd_2Fe_{14}B$, but the manufacture of homogenous Fe nanoparticles remains challenging.[81,82]

A magnetic refrigeration (MR) technique based on the magnetocaloric effect (MCE) has become a possibility for replacing gas compression refrigeration technology because of its high conversion efficiency, lack of gas pollution, safety, and other advantages.[83] The peculiar magnetic characteristics of rare-earth-based compounds have incomparable advantages in the realm of magnetic refrigeration. Changes in magnetic moiety (ΔS_M) and refrigerant capacity (RC) are the main parameters for evaluating the performance of magnetic refrigeration. ΔS_M in response to variations in magnetic field (ΔH) can directly characterize the MCE. Based on Maxwell's magnetization experiment, eqn (4) establishes the link between temperature (T), ΔH, and ΔS_M.[84]

$$\Delta S_M(T, \Delta H) = \int_0^H \left(\frac{\partial M(H,T)}{\partial T}\right) dH \quad (4)$$

RC is calculated from eqn (5):[85]

$$RC = \int_{T1}^{T2} |\Delta S_M| dT \quad (5)$$

where $T1$ and $T2$ represent the temperature at $\frac{1}{2}|\Delta S_M^{max}|$ on both sides of the $-\Delta S_M(T)$ curve.

In the following sections, $RECrO_3$ is used as a study object to show how rare earths can be used in the field of magnetic refrigeration. Magnetic phenomena, such as temperature-induced magnetization reversal and temperature-induced magnetization hopping, were reported in the $RECrO_3$ system due to the presence of RE–RE, RE–Cr, and Cr–Cr magnetic interactions.[86] Fig. 2 depicts both the crystal structure and the spin structure of $RECrO_3$. Yin *et al.* synthesized single crystals of $RECrO_3$ (R: Dy, Tb, Er) *via* a solvent method.[86,87] The relationship between the magnetization and temperature (M–T) of $RECrO_3$ (R = Dy, Nd, Tb, Er) crystal and the evolution of the crystal's spin structure along various axes is depicted graphically in Fig. 3a–d. The Cr^{3+} in each $RECrO_3$ crystal exhibits magnetic anisotropy within a particular temperature range. In terms of magnetization anisotropy, $RECrO_3$ (R = Dy, Nd, Tb, Er) demonstrates a notable degree of anisotropy (Fig. 4a–d). These findings are congruent with those of prior research. Interestingly, Fig. 5a reveals that the decrease in $NdCrO_3$ magnetization along the c-axis (M_c) coincides with the increase along the a-axis (M_a), a phenomenon that persists even in the presence of a 3 T magnetic field. On the saturation magnetization–magnetic field (M–H) relationship curve of the $TbCrO_3$ crystal (Fig. 5b), a unique behavior of stepwise magnetization rise can be observed. Even in the absence of a magnetic field, the original curve demonstrates stepwise growth, demonstrating that this is a unique attribute of the $TbCrO_3$ crystal itself. The magnetic moiety (ΔS_M), maximum magnetic moiety (ΔS_M^{max}), and refrigerant capacity (RC) of $RECrO_3$ were computed using eqn (4) and (5), and the results are presented in Table 4. This work describes how the rare earth affects the spin effect of $RECrO_3$ and the two-step-up behavior of saturation magnetization. This suggests that the $RECrO_3$ system has great magnetic anisotropy and magnetocaloric properties and could be used for magnetic refrigeration.

Despite having stronger magnetic characteristics than nickel–cobalt alloys, ferrite, and steel magnets, the recovery of rare earth magnetic materials is a significant obstacle to the long-term sustainable use of rare earths.[88] The separation stage is a crucial processes that impacts the recovery efficiency. At the moment, leaching for chemical separation using hydrometallurgy is a particularly efficient approach for separating rare earth elements. Sarfo *et al.* used a novel hydrometallurgical process to recover rare earth magnet scrap, which consisted of H_2SO_4 leaching, NH_4OH precipitation and $NH_4F \cdot HF$ reaction.[89] The magnet scrap was converted into rare earth fluoride, which was then converted into rare earth metals by high-temperature calcination. The process of this work not only avoids the use of hydrofluoric acid, but also optimizes the process through statistics and modeling to achieve high-purity rare earth resource recovery, which lays a solid foundation for the sustainable development of rare earth magnetic materials.

Table 3 Research on $Nd_2Fe_{14}B$-based composites utilized in permanent magnets[77–82]

Material	Preparation	Coercivity	Reference
$Nd_2Fe_{14}B$	R-D process	10 KOe	77
$Nd_2Fe_{14}B$	High-energy ball milling	8 KOe	78
$Nd_2Fe_{14}B$	Mechanochemical processing	12 KOe	79
$Nd_2Fe_{14}B$	High-energy ball milling	6.8 KOe	80
$Nd_2Fe_{14}B$/α-Fe	Thermal decomposition, annealing	12 KOe	81
$Nd_2Fe_{14}B$/α-Fe	Microwave assisted combustion process	9 KOe	82

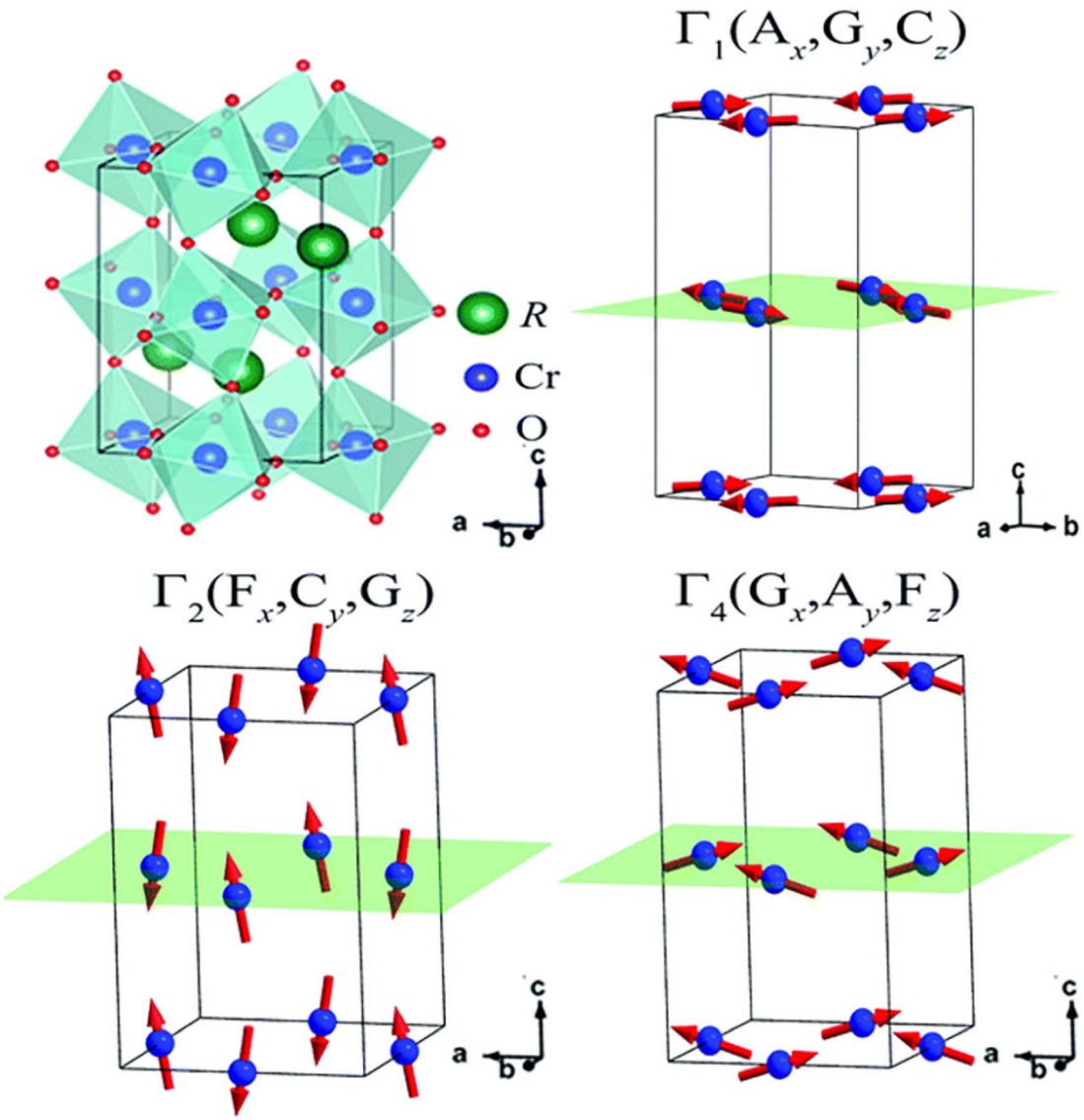

Fig. 2 The crystal and the spin structures of $RECrO_3$.

2.2.3 Rare earth luminescent materials. The luminescence of rare earths is dependent on the transition of 4f electrons between the f–f and f–d configurations. Rare earth elements can emit light across the entire spectrum of wavelengths due to their unique electronic layer structure, abundant ion energy levels, and peculiar transitions of 4f electrons.[90] The electronless Sc^{3+}, Y^{3+}, and La^{3+} and the electron-filled Lu^{3+} of the 4f orbital have a closed shell; hence they are optically inert and can be utilized as the matrix of optical materials.[91] The remaining 13 rare earth ions with un-full electron-filled 4f orbitals, represented by Ce^{3+}, can emit light *via* 4f electron transitions.[92] Consequently, they are suitable as luminous materials for activating ions. Awareness of the optical characteristics and microstructure of rare earth luminescent materials has reached a new level as a result of their widespread application and in-depth research.[93,94] It is vital to understand the mechanism of rare earth luminescence before elucidating the mechanism of rare earth luminescence. For lanthanides, the electron–electron interaction is stronger than the spin–orbit interaction, but the spin–orbit coupling constant is considerably larger; hence the Russell–Saunders coupling equation is still utilized. The Hamiltonian (H) operator expression is as follows:[95]

$$H = \sum_{i=1}^{n} \frac{h^2}{8\pi^2 m} \Delta i - \sum_{i=1}^{n} \frac{ze^2}{r_i} + \sum_{i>j-1}^{n} \frac{e^2}{r_{ij}} + \sum_{i=1}^{n} \xi(r_i) s_i l_i \qquad (6)$$

where ze is the amount of charge, n is the number of electrons, m is the electron mass, i is the Laplace operator, h is the Planck constant, and ξ is the spin–orbit coupling constant.

Rare earth luminescent materials (RELs) can be divided into different excitation methods: cathode ray, photoluminescence, electroluminescence, X-ray luminescence, thermoluminescence, and laser materials, *etc.*[96] They have the incomparable advantages of radiation resistance, resistance to light decay, good temperature resistance, high visual efficiency function value, high color purity, *etc.*, and are thus widely used in

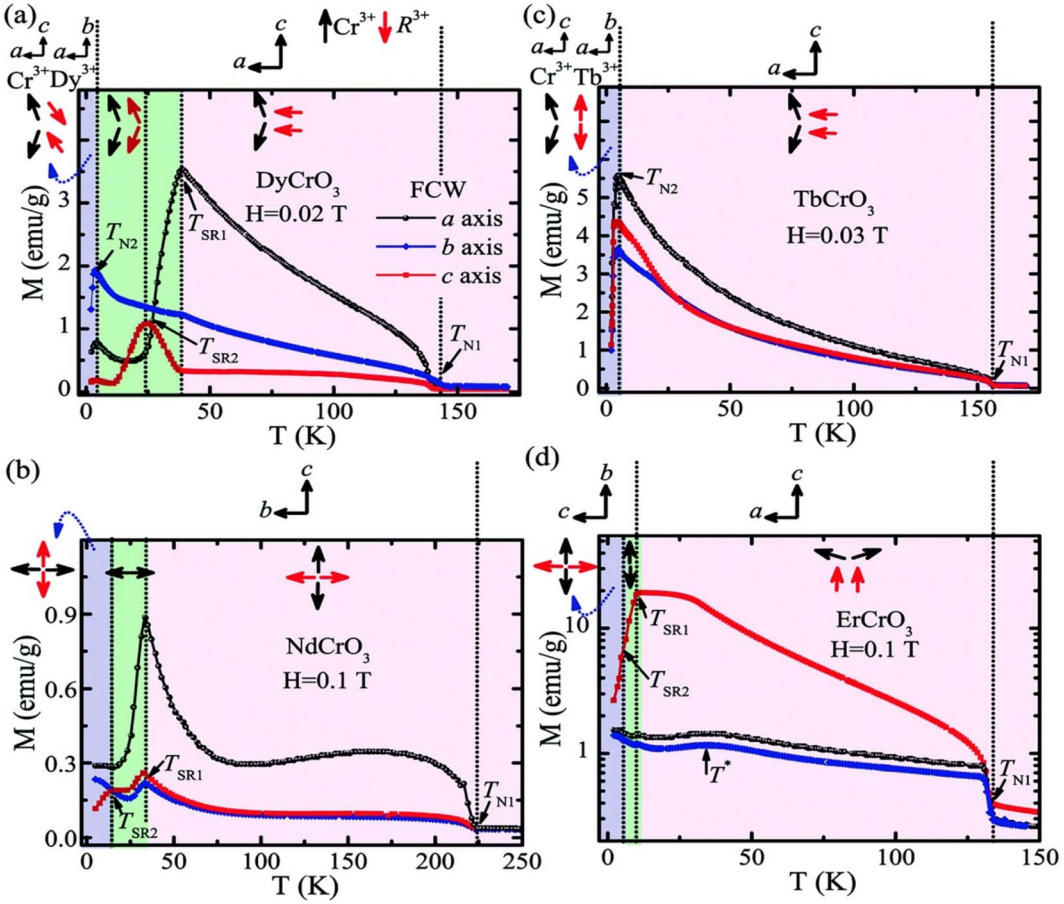

Fig. 3 The relationship between the magnetization and temperature of the $RECrO_3$ crystals and the evolution of the crystal's spin structure along various axes.

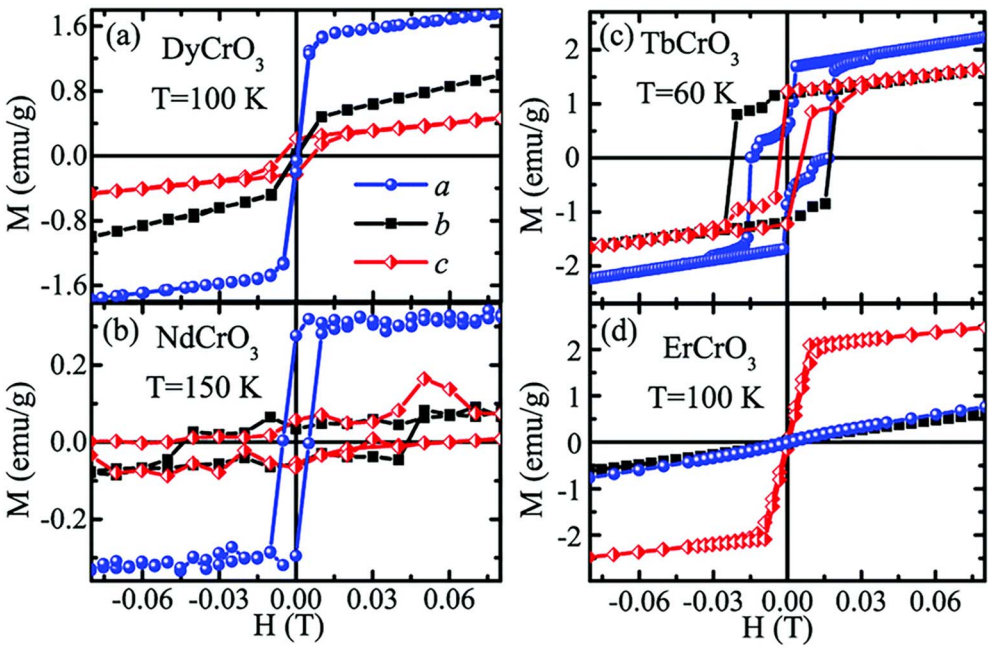

Fig. 4 The isothermal magnetic field dependency of different axial directions of $RECrO_3$ crystals.

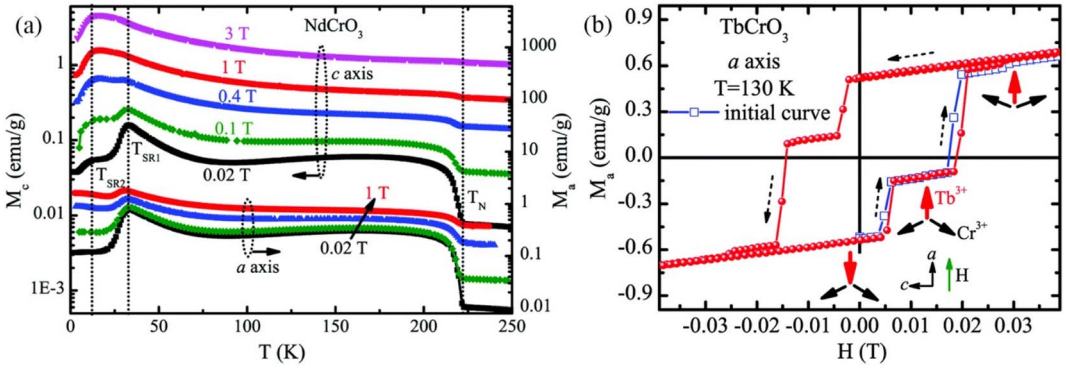

Fig. 5 Schematic illustration of the isothermal magnetization and corresponding spin structure evolution of $RECrO_3$ and $TbCrO_3$ crystals: (a) the isothermal magnetic field dependency of different axial directions of $RECrO_3$ crystals, (b) the evolution of the isothermal magnetization and related spin structure of $TbCrO_3$ crystals is depicted *via* a schematic.

Table 4 The magnetic parameters of $RECrO_3$ crystals[87]

	$-\Delta S_M$ (J Kg K)		$-\Delta S_M^{max}$ (J Kg K)		
Material	$\Delta H = 2T$	$\Delta H = 4.5T$	$\Delta H = 2T$	$\Delta H = 4.5T$	RC (J Kg^{-1})
$DyCrO_3$	11.5	15.2	11.4	14.8	300
$NdCrO_3$	−0.2	−1.1	—	—	—
$TbCrO_3$	5.0	12.2	0.7	5.4	125
$ErCrO_3$	10.1	20.6	9.5	16.9	276
$GdCrO_3$	14.1	31.6	4.3	3.8	—

lighting, display, radiology, national defense, and other fields. Eu^{3+}-activated YVO_4, Y_2O_3, and Y_2O_2S are currently the most efficient cathode-ray luminous materials, replacing the original Mn^{3+}-activated $Zn_3(PO_4)_2$ used in TVs, greatly improving the distortion of TV images, brightness–current saturation, and other characteristics, a leap forward in the color TV industry.[97] With in-depth research into rare earth trichromatic (red, blue, and green) phosphors, rare earth photoluminescent materials have been rapidly developed. Y_2O_3:Eu^{3+}, with quantum efficiency of up to 100%, is nearly ideal for red phosphors; Tb^{3+} is mostly chosen as the activating ion for green phosphors. For use of $^5D_4$–^7F_j energy level transition luminescence, subsequent research proved that doping with sensitizer Ce^{3+} can achieve radiation-free energy transfer between Ce^{3+} and Tb^{3+}, greatly improving the luminous efficiency.[98,99] Currently developed rare earth electroluminescent materials (RE-EL) are mainly Eu^{2+} and Ce^{3+} activated CaS or SrS, where the CaS or SrS matrix allows high-energy electron transport inside the crystal. Eu^{2+} and Ce^{3+} based on $(4f)^{n-1}5d$–$(4f)^n$ transitions preserve structural stability at high electric field intensities; therefore CaS:(Eu^{2+}/Ce^{3+}) and SrS:(Eu^{2+}/Ce^{3+}) should in future realize the unique color luminescence potential of RE-EL.[100,101] For rare earth laser materials, garnet-type Nd^{3+}-activated yttrium aluminum garnet (YAG:Nd^{3+}) with a narrow fluorescence spectral line, low threshold, and high power has shown the best performance. Nd^{3+} single replacement of Al^{3+} in the lattice in YAG, where the emission spectrum can broaden uniformly, is currently the best option for laser guidance, laser ranging, laser medical treatment, and other fields.[102] A variety of non-linear optical crystals have been made to meet more civilian and military laser needs. Fig. 6 shows the crystal structure of the currently used RE-sulfide (RE-S).[103] Fig. 6a shows the crystal structures of 0-dimensional $Ln_8Sb_2S_{15}$; Fig. 6b–d represent the 1-dimensional structures including Ln_4GaSbS_9, $Ln_3M_xT_yS_9$, and Ba_2InYSe_5; Fig. 6e and f show the crystal structures of 2-dimensional $Eu_2Ga_2GeS_7$ and $EuCdGeQ_4$; and Fig. 6g and h depict the crystal structures of 3-dimensional Ln_3GaS_6 and La_2CuSbS_5. The RE-S active group is extremely distorted and can greatly raise the second harmonic generation (SHG), but the band gap does not surpass the 3 eV threshold. The combination of RE with other reactive groups X–O (X = P, B, C and N) enables tuning of the band gap and SHG effects to achieve optimum laser performance. Subsequent studies discovered that the unique synergy between the RE-S and B–O/C–O groups improved SHG effects and widened the band gap. Future research on RELs should therefore concentrate on rare earth borides and rare earth carbides.

RELs have become a pillar material in the display, lighting, and optoelectronic industries, and their continual development and organic integration with other fields of technology has resulted in the development of new high-precision technologies and industries.[104] Nevertheless, it is indisputable that the direct excitation of RE^{3+} ions is a relatively inefficient luminescence process due to forbidden jump of the rare earth ion 4f jump and the quenching promoted by the –OH, –NH and–CH bond vibrations in the adjacent ligands.[105] Development of quantum dots with exceptional electronic characteristics could provide a remedy. Wang *et al.* synthesized SnS and SnS: Ce^{3+} quantum dots and used the density generalized first principle to compute the energy band structure, total density of states (TDO), and partial density of states (PDO); the findings are depicted in Fig. 7a–d.[106] The spin polarization caused by Ce ions was analyzed using the spin density distribution (Fig. 7e and f), and for the $Sn_{36}S_{36}$, the majority of the spin density is located on S, yet that of $Sn_{36}Ce_1S_{36}$ is found on the Ce ions. The energy level provided by the 4f orbital of the Ce ions effectively promotes the electron jump, and the strong coupling between the carrier and

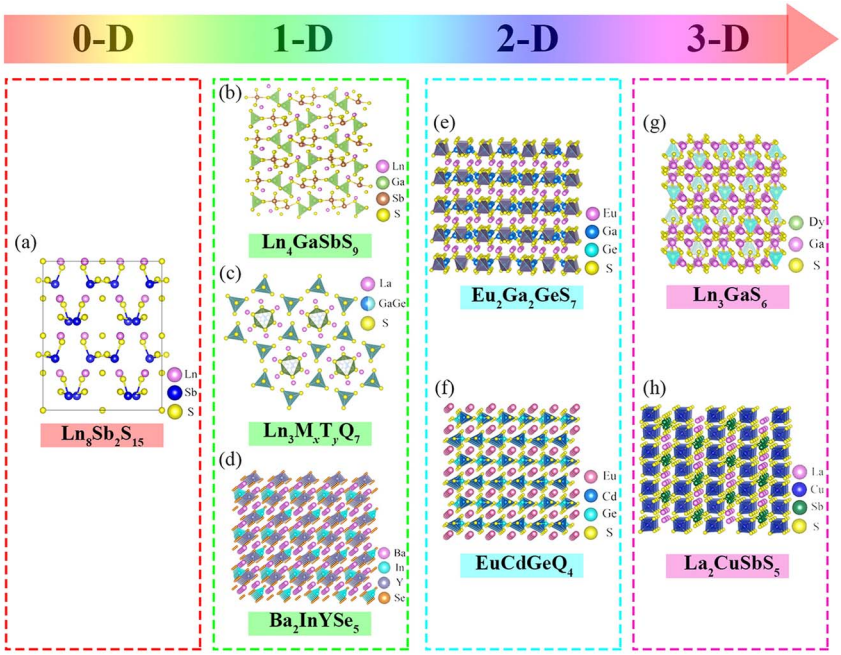

Fig. 6 Schematic diagram of the structure of rare earth sulfides.

the 4f state considerably boosts the photoluminescence intensity of the SnS quantum dots.

In addition to quantum dots, researchers are becoming increasingly concerned with the potential uses of quantum wires, superlattices, and ordered nanostructure arrays.[107,108] Most of the research going on right now is about how quantum confinement and quantum scale affect the structure of energy bands and spectral features. New methods for the preparation of rare earth luminous materials should be developed and studied in the future, beginning with the materials' preparation and processing. For instance, microwave sintering, ultrasonic dispersion, and further synthesis processes will be integrated to promote the development of rare earths in the luminescence field.

2.2.4 Rare earth catalytic materials. The 4f electrons of rare earth elements are shielded by 5s and 5p electrons, and their activity is lower than that of transition metal elements. Hence, rare earth elements are frequently employed as cocatalysts in catalyst systems.[109] However, rare earth catalysts possess a wide variety of catalytic properties, such as the electrocatalytic-based hydrogen evolution reaction (HER), oxygen evolution reaction (OER), oxygen reduction reaction (ORR), catalytic-based CO_2 methanation reaction (CMR), ammonia synthesis reaction (ASR), and a number of other reactions, and their chemical stability and thermal stability are considerably greater than those of other catalysts.[110–112] Therefore, rare earths have vast application potential in numerous organic and inorganic chemical industries.

As the industrialization process accelerates, volatile organic compounds, such as automotive exhaust and formaldehyde, are polluting the atmosphere more and more.[113] Strictly regulating the emission of volatile organic compounds is a significant environmental concern. Due to its low flame-out temperature, consistent combustion, high efficiency, and high-temperature oxidation resistance, rare earth–precious metal oxidation catalysis has been extensively investigated in comparison to other methods for removing organic compounds.[114,115] As illustrated in Fig. 8a, Hu *et al.* fabricated Pt-deposited CeO_2 nanospheres (Pt-CeO_2-NS) and nanorods (Pt-CeO_2-NR) as catalysts and evaluated the reaction mechanism of Pt-loaded CeO_2.[116] CeO_2 considerably improves the catalytic activity for the CO reduction of NO, while Pt provides the NO conversion activity. Compared to rod-shaped CeO_2, spherical CeO_2 contains more oxygen vacancies and demonstrates a stronger interfacial interaction with Pt particles, which further stimulates the surface reaction sites and effectively lowers the CO poisoning effect of platinum. Jiang's investigation revealed the Frankel oxygen vacancy as the crucial active site for catalytic oxidation.[117] MnO_x–CeO_2 produced by the sacrificial template approach possesses exceptional catalytic oxidation performance for ethyl acetate (T_{99} = 210 °C, which is the temperature required for 99% conversion), and Fig. 8b depicts the catalytic oxidation mechanism. In rare earth–precious metal catalysts, the rare earth can enhance the oxygen storage capacity and lattice oxygen reaction activity of the catalyst, promote the uniform dispersion of precious metals on the carrier, and increase the catalytic efficiency, while decreasing the amounts of precious metals needed.

Furthermore, rare earth catalysts play an important and wide-ranging role in making and breaking down ammonia. Ammonia (NH_3) is the primary source of nitrogen fertilizer and nitrogen compounds used in agriculture, and its synthesis is depicted in eqn (7).[118] It is thermodynamically reactive, but because N_2 is an inert gas, it is difficult to obtain the kinetic conditions of ammonia synthesis at low temperatures.[119]

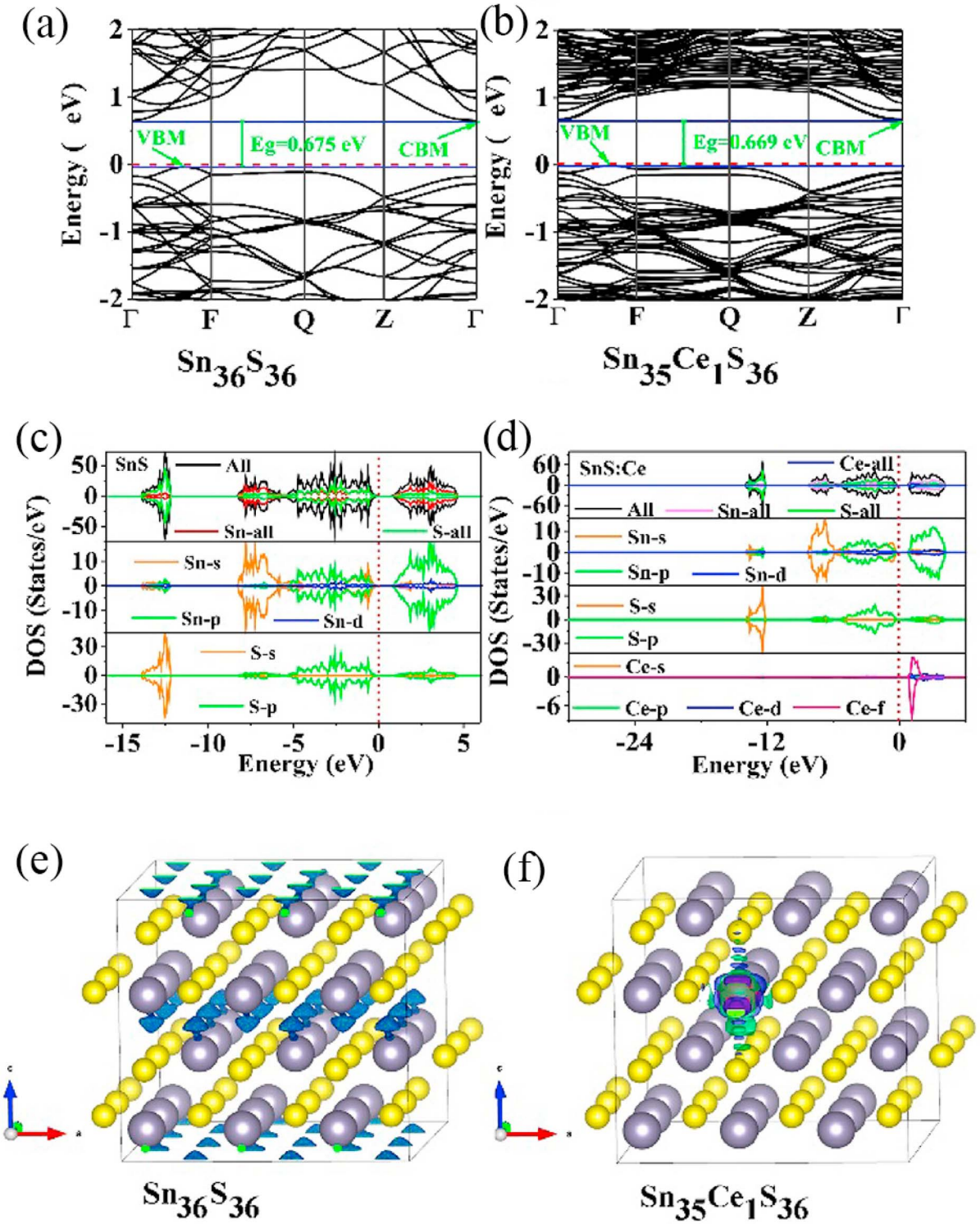

Fig. 7 Band structures of the structural models of SnS ($Sn_{36}S_{36}$) and SnS: Ce^{3+} ($Sn_{35}CeS_{36}$): (a and b) energy band diagrams, (c and d) total and partial density maps, (e and f) spin density maps.

Therefore, scientists are committed to inventing catalysts that facilitate ammonia synthesis:

$$N_2 + 3H_2 \rightarrow 2NH_3 \quad (7)$$

Currently, molten iron catalysts still occupy an absolute position in ammonia synthesis, and it has been found that their activity decreases when the *R*-value (Fe^{2+}/Fe^{3+}) is higher or lower than 0.5.[120] This led to a broad consensus among researchers that the composition of molten iron catalysts is set, and that

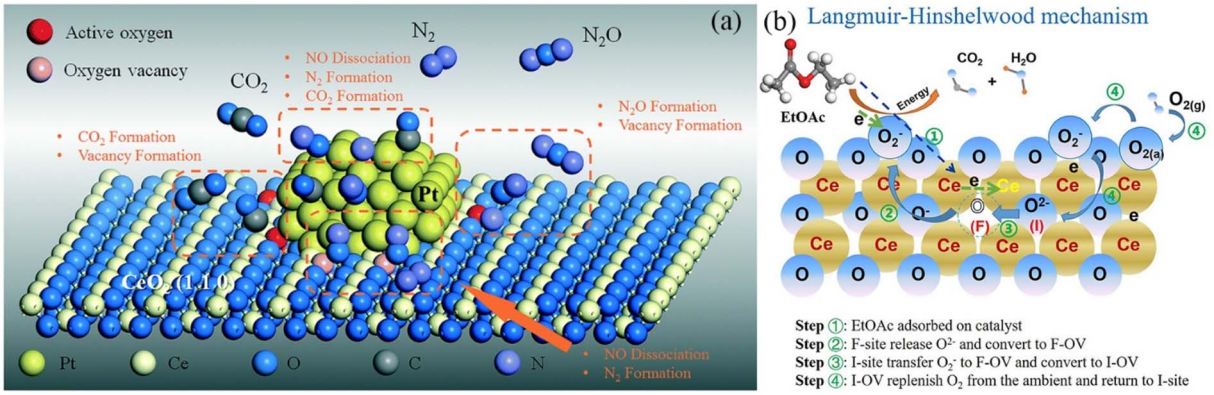

Fig. 8 Catalytic reaction mechanism of rare earth catalysts: (a) reaction mechanism of CO reduction of NO with Pt/CeO_2-NR catalyst, (b) catalyzed oxidation processes mediated by Ce-based catalysts.

consequently changing the composition would not improve the catalytic performance of such catalysts. The classical theory that the catalytic activity is optimal at an *R* value of 0.5 for molten iron catalysts was followed for more than 80 years until a new cobalt-containing molten iron catalytic system with better performance was found to break this classical conclusion.[121] Cobalt-containing catalysts are an important development of traditional Fe-based fused iron catalysts, marking a new period of development for ammonia catalysts. ICI (UK) first successfully developed an Fe–Co catalyst (type 74-1 containing drill catalyst), which led to a certain improvement in its activity and was applied in the ICI-AMV process. China has also successfully developed Fe–Co catalysts (type A201 and A202) and applied them to industrial production with good production benefits.[122]

In 1976, Takeshita was the first to discover that rare earth intermetallic compounds absorb hydrogen faster, indicating that they have increased catalytic activity for the dissociation of hydrogen molecules and for diatomic molecules such as N_2.[123] Compared to commercially available iron catalysts with high cobalt content, the use of rare earth blends can reduce the cobalt content or even replace it completely, which significantly reduces the cost of molten iron catalysts. Subsequently, Niwa discovered in 1998 that the rare earth element La had a considerable impact on the ammonia synthesis activity of MgO-supported ruthenium.[124] And noble metal catalysts doped by rare earth composite oxides demonstrated superior catalytic performance in terms of reactivity, selectivity, and stability under high-temperature settings. Since then, rare earth catalyst research has entered a new era. Okura investigated the effects of various rare earth oxide supported Ni catalysts on the breakdown of ammonia.[125] In a study of reaction kinetics, rare earth oxide supports can effectively ameliorate the phenomenon of hydrogen inhibition in the reaction process. The Y_2O_3–Ni catalyst shows the highest catalytic activity at elevated temperatures, and research indicates that the optimal Ni loading is 40% (wt%), and Ni can be supported uniformly on the Y_2O_3 carrier under these conditions. Moreover, the perovskite-type rare earth composite catalyst showed outstanding reaction kinetics during ammonia production. Li produced $BaCeO_3$ modified with rare earth elements (La, Y, Pr), and the ammonia synthesis rate of $BaCe_{0.9}La_{0.1}O_{3-\delta}$ supporting 5% Ru at 3 MPa and 450 °C was as high as 34 (mmol (g^{-1} h^{-1})), with no loss of catalytic performance after 100 h of continuous reaction.[126] The addition of La^{3+} increases oxygen vacancies in the lattice and decreases the particle size of Ru, which is advantageous for the increase in electron density on the Ru surface and the production of more b5-type active sites that promote N–N dissociation.

In conclusion, the ammonia synthesis reaction is of high industrial importance and the fused iron catalyst has excellent properties that cannot be matched by some other ammonia synthesis catalysts.[127] However, in achieving the sustainable development of materials and processes, the aim is to minimize the consumption of non-renewable resources and the negative impact on the environment. In addition, minimizing dependence on a particular raw material is essential to sustaining high-tech industries and maintaining economic progress.[128] Considering the non-renewable nature of iron-bearing ores and the cost of Co resources, a logical step for the industrial economy is to promote the substitution of reserve-rich, environmentally friendly and low-cost rare earth resources, and therefore research and development of rare earth catalysts is crucial for the current and future ammonia industry to comply with the concept of sustainable green development.

2.2.5 Rare earth energy storage materials. The sustainability of the energy supply and tackling the problem of environmental contamination are difficult problems that today's and future society must face.[129] In light of the current situation of rising energy demand and worsening environmental pollution, the development of new sustainable energy sources has emerged as a high priority in the energy industry. Due to its high calorific value (120 MJ kg^{-1}) and lack of pollutants, hydrogen energy is currently the best alternative to nonrenewable energy sources such as fossil fuels.[130] Hydrogen can be utilized as an energy carrier to complement intermittent energy release from renewable energy sources, such as wind energy and solar energy. Additionally, hydrogen can be exploited directly as a heat source, with fuel cells or internal combustion engines converting it to power or heat.[131] However, the conventional method of storing hydrogen in gas cylinders is inefficient and prone to leakage. Thus, the best and safest way to store

hydrogen to date, solid-state hydrogen storage, is being looked into.[132] Solid-state hydrogen storage materials allow for safe and efficient transportation, and many studies have been conducted on solid-state hydrogen storage materials.[133,134]

Among the various candidate materials for hydrogen storage, ionic hydrides (*e.g.* LiH and MgH_2 based on first and second main group elements) are gaining interest due to their high hydrogen storage capacity (7.7 wt%), low raw material cost, and great cycle reversibility.[135,136] There are downsides, however, such as poor hydrogen absorption and discharge kinetics, high operating temperature, and poor stability in air. From a practical standpoint, such hydrogen storage materials require further improvement in terms of hydrogen discharge temperature, hydrogen discharge rate, and reversible hydrogen storage performance, and the strong chemical bonding interactions between the atoms of constituent elements in Li- and Mg-based hydrides present significant thermodynamic and kinetic challenges for hydrogen storage applications.[137,138]

Against the backdrop of contemporary research on hydrogen storage, AB_5-type (A: RE metal, B: transition metal) RE-based alloys exhibit exceptional performance. The hydrogen storage capacity of $LaNi_5$ is as high as 190–200 $cm^3\ g^{-1}$.[139] It features easy activation, a moderate equilibrium pressure, minor hysteresis, rapid hydrogen absorption and desorption rates, and nontoxicity, so it has become a representative hydrogen storage material of high quality.[140] Since 1970, when Van Vucht first documented the behavior of $LaNi_5$ reversibly absorbing and releasing hydrogen at ambient temperature,[141,142] $LaNi_5$ hydrogen storage materials have experienced fast growth. Due to the limitations of the initial experimental conditions, it is difficult to set up a prolonged isothermal reaction; hence, there are a variety of differing opinions regarding the primary factors governing the reaction kinetics of $LaNi_5$: I. it is controlled by the chemical reaction of hydrogen atoms with the α-phase solid solution at the two-phase interface.[142] II. It is controlled by the diffusion of hydrogen molecules in the beta phase.[143] III. There is chemisorption control of hydrogen molecules on surfaces.[144] IV. Controlled variables fluctuate with degrees of response.[145] On this basis, Silin *et al.* systematically studied the reaction kinetics of $LaNi_5$ hydrogen storage by the two-phase coexistence initial rate method. They assumed that $LaNi_5$ was a spherical particle with a constant density before and after hydrogenation; the reaction's apparent activation energy is 4700 cal (g^{-1} mol^{-1}), and the reaction rate equation is as follows:[146]

$$\frac{dX}{dt} = 64.33(p - p_{eq})\exp(-4700/RT) \quad (8)$$

Knowing that $p_{H_2} = p_0$, $p_{H_2}{}^{eq} = p_{eq}$, $X = \frac{n_h}{n_f}$, represents the ratio between the amount of hydrogen absorbed (n_h) and the entire amount of hydrogen that can be absorbed in the two-phase zone (n_f). This model correlates well with the kinetic data of $LaNi_5$ during the reaction process, demonstrating that the chemisorption of hydrogen molecules on the alloy's surface is the primary factor governing the kinetics of the hydrogenation reaction. However, $LaNi_5$ undergoes a substantial volume expansion of 23.5% during the hydrogen absorption and desorption process, and the usage of pure metal as a raw material is expensive, hence limiting its implementation on a broad scale in the field of hydrogen storage.[147] Therefore, further research focuses primarily on three aspects: enhancing reaction kinetics, cycle stability, and cost reduction.[148] The internal stress caused by the volume expansion and contraction of $LaNi_5$ during the hydrogen absorption and desorption processes will damage the material's internal structure, and the newly exposed surface will be oxidized to form an impurity phase, which hinders the hydrogen absorption and desorption processes. Adding polymer to form composites is the optimal solution for resolving this problem of cycling stability.[149] The existing series of LMBNH-TPX, LMNH-TPX,[150] Mg-NCs/PMMA,[151] Mg-PMMA,[152] SP-MnO_6,[153] SPMnO_2 (A, B, E)[154] alloy-polymers provides a good barrier for hydrides, preventing oxidation and corrosion of the material, considerably increasing the reversible cycle life, and inhibiting side reactions of metal hydrides during hydrogen absorption and dehydrogenation reactions. By ball milling and wet milling, Almeida Neto *et al.* made BM-AES/$LaNi_5$ and WM-AES/$LaNi_5$ composites with AES-polymer-doped $LaNi_5$.[155] The molten BM-AES/$LaNi_5$ was generated into filaments signified as P-AES/$LaNi_5$, and the preparation procedure is depicted in Fig. 9a. Fig. 9b(1 and 2) depict the sample's short- and long-term hydrogen absorption capacity. AES-$LaNi_5$ has the best hydrogen absorption kinetics. P-AES/$LaNi_5$ has a poor short-term capacity for hydrogen absorption, but after 12 h, its hydrogen capacity is comparable to that of other samples. The changes in hydrogen capacity during cycling are depicted in Fig. 9c(1 and 2). All samples exhibited a declining and then stabilizing trend. During cycling, defects that trap hydrogen atoms in the hydride structure may account for the loss in capacity. In sum, this study demonstrates that $LaNi_5$ particles with superior particle dispersion have superior hydrogen storage capabilities. Adding AES can effectively increase the performance of the composite's hydrogen absorption/dehydrogenation cycle and prevent the negative effect of air on the kinetics of hydrogen uptake.

To lower costs, mixed rare earth elements (La, Ce, Pr, Nd) are used to replace high-valent La,[156,157] and Al, Mn, Cr, Fe, and Co are used to replace Ni. In these investigations, it has been discovered that the stability of hydrides can be enhanced without incurring any capacity loss. Increasing the amount of Ce and Pr in a misch metal can accelerate reaction kinetics and improve temperature stability. In contrast, the presence of a lot of La and Nd decreases the performance. The mixed rare earth $RENi_5$ with the ratio $La_{0.1645}Ce_{0.7277}Pr_{0.0234}Nd_{0.0845}Ni_5$ has the highest hydrogen storage capacity, according to numerous experiments.[158–161] Al and Mn partially replacing Ni can boost cycle stability and decrease reaction equilibrium pressure; Fe, Co, and Cr can partially replace Ni to increase hydrogen storage capacity, as Fe, Co, and Cr exhibit greater electron attraction and considerably increase the number of hydrogen atoms.

The aforementioned research strategies are efficient in enhancing the hydrogen storage performance and reducing the cost of RE-based alloys, but they are insufficient to suit the needs of practical industrial applications. To further enhance

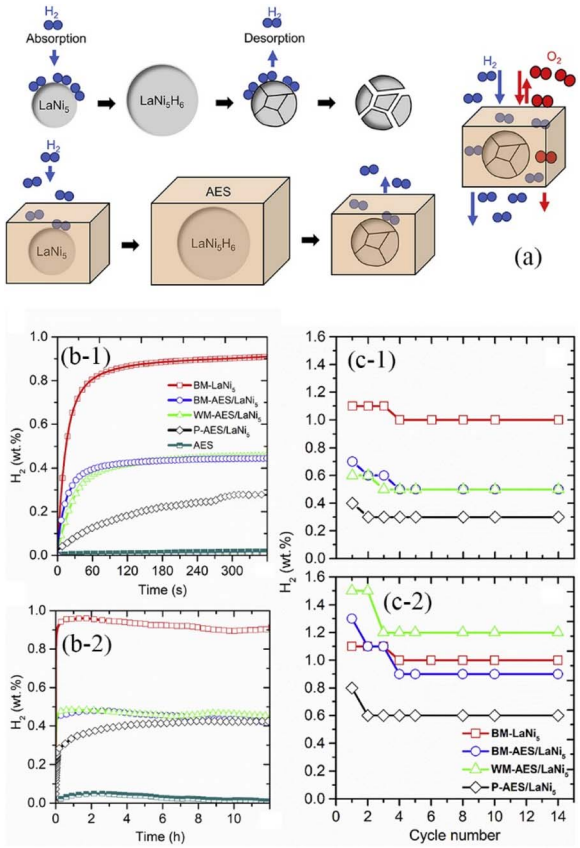

Fig. 9 Flowchart of the preparation and hydrogen absorption content cycle stability: (a) diagram illustrating the transformation of BM-AES/$LaNi_5$ into filamentous P-AES/$LaNi_5$, (b-1) hydrogen absorption of different samples within 300 s, (b-2) hydrogen absorption of different samples over 10 h, (c-1) cyclic stability diagram of actual hydrogen content, (c-2) hydrogen content cyclic stability diagram for the initial absorption phase.

the hydrogen storage capacity as well as the kinetics and thermodynamics of rare-earth-based compounds, the following modification methods can be used: nanosizing, synthesizing sub-stable phases, doping with catalytic additives, forming nanocomposites, changing the reaction mode, *etc.*[162] However, it is important to note that none of the aforementioned modification techniques can entirely meet the requirements of real applications. Doping, synthesis of sub-stable phases, and altering the reaction path, for instance, can effectively reduce the enthalpy of generation; however, not all reactions are totally reversible, resulting in a lower hydrogen storage capacity.[163] Although rare earths still face serious challenges in the practical application of hydrogen storage, they offer a new idea in the development of hydrogen storage materials.

In light of the existing limitations associated with hydrogen energy storage and the intermittent release of energy from renewable energy sources, it is vital to create new and efficient energy storage devices, among which lithium-ion batteries (LIB) and supercapacitors are representative.[164–166] In electrochemical energy storage, RE-based compounds also show amazing promise. Typically, rare earth elements are doped in LIB to modify the electrodes (common ones are $LiCoO_2$ and $LiMn_2O_4$).[167,168] The large-radius rare earth ions are introduced into the lattice of the electrode material to induce distortion, thereby decreasing the charge transfer resistance and enhancing the electrode material's conductivity.[169,170] $LiCoO_2$ is a common cathode material for LIB with a theoretical specific capacity of up to 274 mA h g^{-1}. It is currently the cathode material with the highest compaction density and thus the manufactured lithium-ion battery has the largest volume specific energy, and it has become the primary material for batteries used in tablet computers and mobile smart terminals.[171] However, when the voltage exceeds 4.35 V, $LiCoO_2$'s capacity diminishes dramatically.[172] The highest capacity of commercial $LiCoO_2$ is therefore just 165 mA h g^{-1}. Liu *et al.* fabricated $LiCoO_2$ doped with La and Al (D-LCO) *via* liquid-phase crystallization; the structure diagram is shown in Fig. 10a.[173] La functions as a pillar to support the structure and suppress the phase transition during cycling. Al, on the other hand, acts as a charge center to allow Li to diffuse even at 4.5 V. When D-LCO was charged to 4.5 V, three distinct phase transitions of Li/Li^+ occurred at 4.1 V, 4.2 V, and 4.46 V along the dQ/dV curves (Fig. 10b). *In situ* testing (Fig. 11a–e) reveals that Li^+ intercalation/deintercalation is extremely reversible and there is no discernible phase transition. The maximum volume change of the P-LCO battery is 3.63%, as depicted in the voltage and volume change curve (Fig. 11f).

$LiMn_2O_4$ is also a typical cathode material for batteries, but the performance degradation brought on by manganese dissolution restricts its practical application.[174] Cationic doping modification can effectively inhibit manganese dissolution, stabilize the surface crystal structure, and produce a protective layer to prevent corrosion by the electrolyte.[175] Ram synthesized $LiMn_2O_4$ doped with various rare earth elements (Gd, Tb, Dy, Yb) using the sol–gel method.[176] According to studies, doping $LiMnO_4$ with Dy and Tb can successfully improve its conductivity, while Gd and Dy can greatly enhance its cycle performance. In a study, Singhal *et al.* improved the cycling stability of $LiMn_2O_4$ by supplementing with Nd.[177] Other cathode materials doping rare earth elements provide a variety of performance enhancements. Doping $LiNi_{0.5}Co_{0.2}Mn_{0.3}O_2$ with Ce, for instance, can increase the initial discharge capacity and cycle stability.[178] Comparative research was conducted on the impact of Y doping on the performance enhancement of $LiMn_2O_4$, $Li_{1+x}V_3O_8$, and $LiFePO_4$.[179] Doping with Y decreases the crystal parameters of $LiMn_2O_4$, increases the (100) interplanar spacing of $Li_{1+x}V_3O_8$, and decreases the grain size of $LiFePO_4$. Various Y doping mechanisms result in distinct performance enhancements. The appropriate amount of doped Y enhances the initial discharge capacity of $LiFePO_4$ and $Li_{1+x}V_3O_8$ as well as the cycling performance of $LiMn_2O_4$.

However, due to the low power density and poor cycle stability of lithium-ion batteries, they will not be able to meet the demand for higher energy consumption, faster power transfer, and higher stability during cycling in the future.[180] Supercapacitors compensate for this deficiency and are being intensively explored.[181] Supercapacitors are divided into electric double-layer capacitors and pseudocapacitors according to their mechanism. The majority of double-layer capacitor electrode

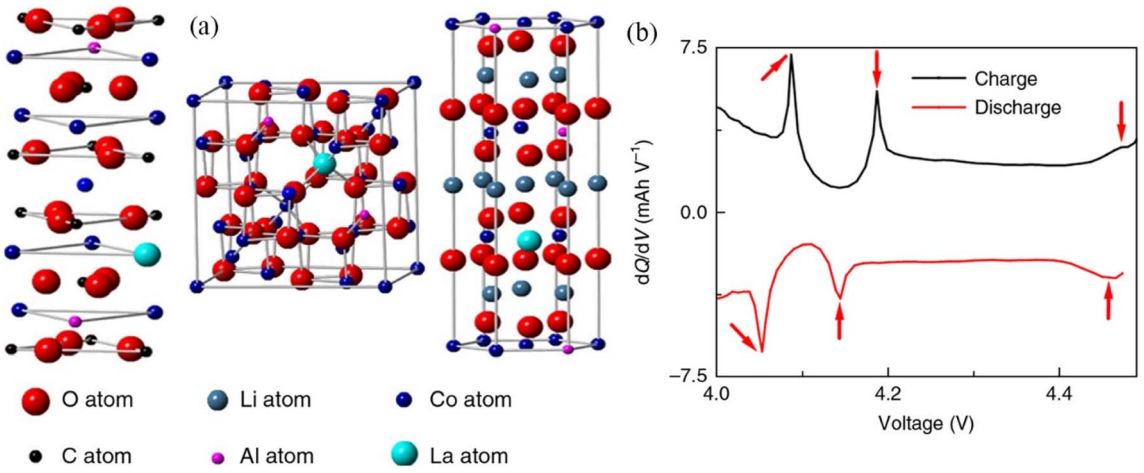

Fig. 10 Structural diagrams and dQ/dV curves: (a) diagrammatic representation of the structures of doped $CoCO_3$ and Co_3O_4, (b) dQ/dV curves of pristine $LiCoO_2$ during charging and discharging.

materials are carbon and carbon derivatives, which are outside the focus of this research. Therefore, the following sections describe the application of rare earths in the field of pseudocapacitors.

3 Pseudocapacitive applications

In the 1960s, David C. Graham used the word "pseudocapacitance" to describe extra electrochemical capacity that is not caused by the formation of an electric double layer. This is where the concept of 'pseudocapacitance' originated.[182] In the early 1970s, B.E. Conway first defined pseudocapacitance in his work. Conway proposed: pseudocapacitance describes an electrochemical mechanism similar to capacitance but is actually a charge transfer process at the electrode–electrolyte interface, a fast and reversible redox reaction, which is the reason for decorating with the prefix 'pseudo'.[183] As illustrated in Fig. 12, the pseudocapacitance mechanism can be broken down into three sub-mechanisms: underpotential deposition, redox, and intercalation pseudocapacitance.[184] According to this description, the pseudocapacitive electrode material and the double layer electric electrode material are clearly defined. Despite the fact that the energy storage behavior of the electric double-layer electrode material also occurs on the surface of the electrode material, the entire process involves only the simple faradaic reaction of charge adsorption.[185,186] The cyclic voltammetry (CV) and galvanostatic charge–discharge (GCD) patterns of pseudocapacitors are comparable to those of EDLC due to the rapid surface or near-surface charge transfer.

However, pseudocapacitive materials that store energy through redox reactions behave like batteries in some ways.[187,188] When the particle size of the cathode $LiCoO_2$ block, which is predominantly used in lithium-ion batteries, reaches the critical nanometer size of 10 nm, the battery characteristics vanish and the voltage distribution transitions from the platform to ramp form, exhibiting miraculous capacitance characteristics.[189] The major difference between pseudocapacitive and battery materials is that pseudocapacitive materials are not constrained by ion diffusion within the electrode material, whereas battery materials are governed by the diffusion process. With an in-depth study of how pseudocapacitance stores charge and the widespread use of nanomaterials and thin-film materials, more and more studies have shown that the pseudocapacitance mechanism and the diffusion process control each other in pseudocapacitive materials.[190] This is due to the fact that nano-scale electrode materials have greater specific surface areas and shorter ion diffusion paths than traditional bulk materials, and this difference can even be of several orders of magnitude, making it increasingly difficult to distinguish between the surface and bulk of materials. This synergistic effect happens not just with traditional battery materials, but also with intercalation materials like TiO_2, Nb_2O_5, metal oxides, MoO_x, MXene, and emerging cationic intercalation materials.[191–194] Therefore, intercalated pseudocapacitance combines the advantages of batteries and supercapacitors, namely massive charge storage and storage that is not governed by diffusion.

In many intercalation pseudocapacitive materials, rare earth compounds have become an important area of study in the past few years.[195] Since rare earth elements are often regarded as electrochemically inactive, abundant rare earth resources have been neglected in the field of pseudocapacitors in previous studies. However, the majority of rare earth elements show RE^{3+}/RE^{2+} or RE^{4+}/RE^{3+} redox coupling, laying the thermodynamic groundwork for their employment in pseudocapacitive energy storage.[196] Rare earth oxides are the largest group of rare earth compounds that are easily manufactured, structurally stable, corrosion-resistant, and harmless to the environment.[197] Their electrochemical activity can be changed by changing the amount of oxygen vacancies and oxygen in the lattice, which is a simple step in the manufacturing process. Thus, rare earth oxides have tremendous practical potential in the pseudocapacitive field.[198] In subsequent sections, we will discuss the application and compound strategies of rare earth oxides in pseudocapacitors in recent years, clarify the energy storage mechanism of rare earth oxides, and provide references for

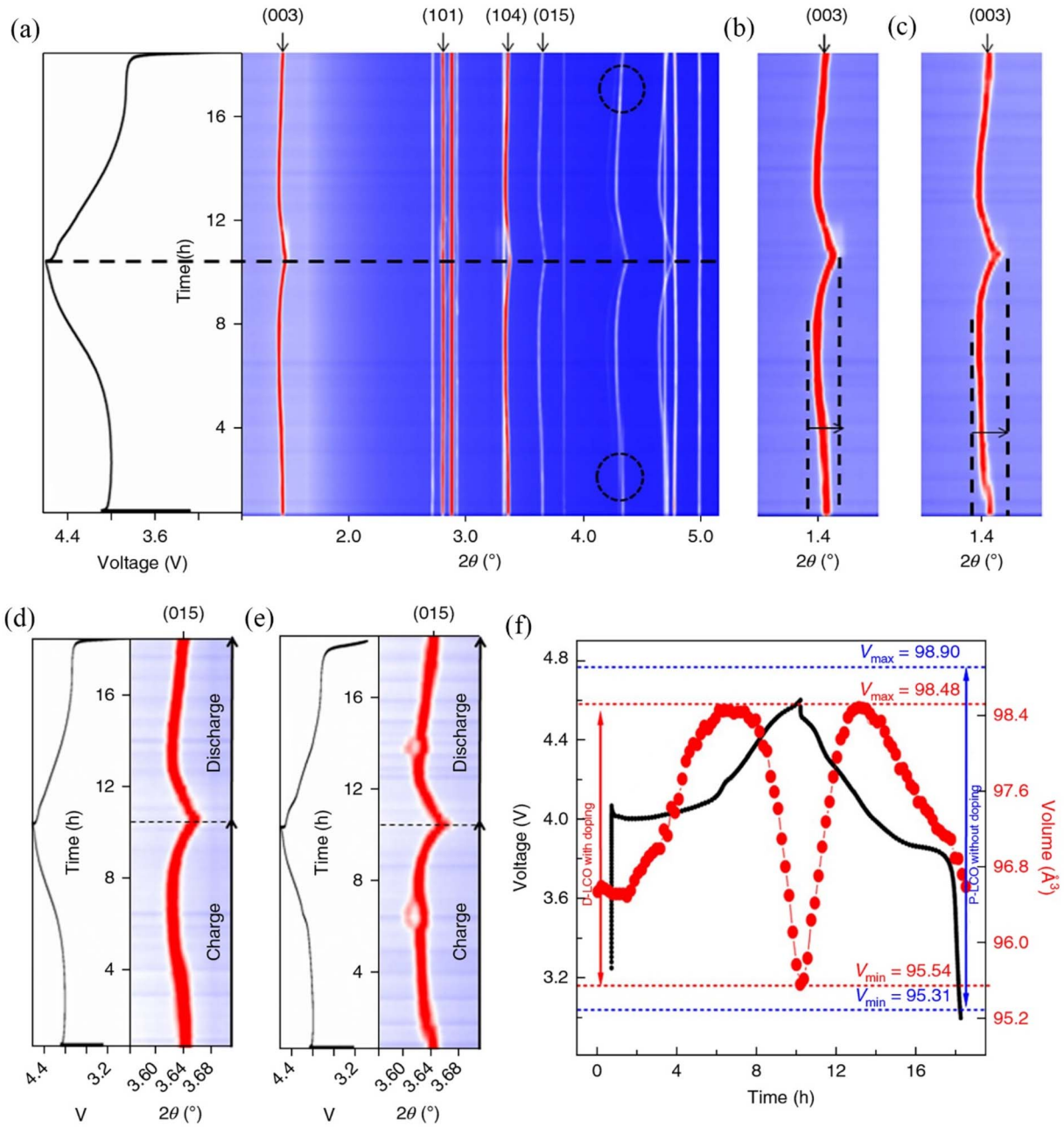

Fig. 11 *In situ* characterization of pristine $LiCoO_2$ (P-LCO) and Co-doped $LiCoO_2$ (D-LCO) first charge and discharge process: (a) voltage distribution and corresponding contour plot, (b) contour plot of (003) evolution of D-LCO, (c) contour plot of (003) peak evolution of P-LCO, (d) contour plot of (015) evolution of D-LCO, (e) contour plot of (015) peak evolution of P-LCO, (f) the voltage distribution of D-LCO (black) and P-LCO (blue), and the volume change process of D-LCO battery (red).

enhancing the performance of rare earth oxide pseudocapacitors.

3.1 Typical oxides for pseudocapacitance

3.1.1 Cerium oxide. CeO_2 is the most typical pseudocapacitive material among rare earth compounds. CeO_2 offers the advantages of environmental protection, plentiful supply, easy preparation, high cost-effectiveness, corrosion resistance, and excellent redox capacitance performance; thus researchers have shifted their attention to study CeO_2.[195,199,200] Table 5 summarizes recent research on CeO_2 as a pseudocapacitive electrode material. CeO_2 belongs to the cubic crystal system and has a fluorite structure. It belongs to the *Fm*3*m* space group. Cerium cations in the CeO_2 unit cell are arranged in a face-centered cubic matrix; oxygen anions occupy all four tetrahedral positions.[201] Cerium cations coordinate with eight neighboring oxygen anions, while oxygen anions coordinate with four nearby cerium cations. The ground state valence of the element Ce is $4f^15d^16s^2$. It loses one 5d and two 6s electrons in order to generate stable Ce^{3+}, and one more 4f electron to form stable Ce^{4+}. Therefore, CeO_2 can realize electrochemical energy

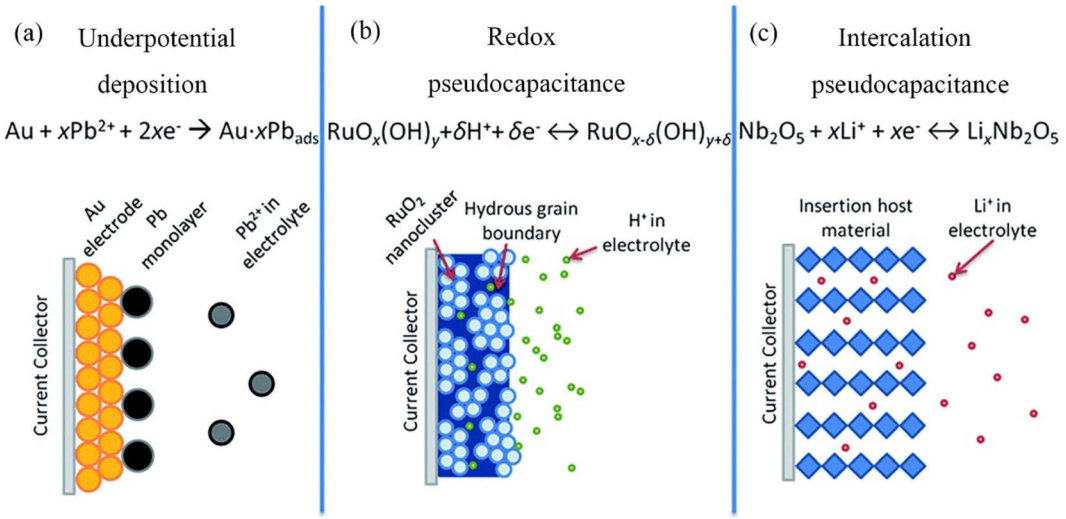

Fig. 12 Different pseudocapacitance mechanisms: (a) underpotential deposition, (b) redox pseudocapacitance, and (c) intercalation pseudocapacitance.

storage *via* the rapid reversible conversion of Ce^{3+} and Ce^{4+}. The charge storage mechanism of CeO_2 electrode material is based on the cation intercalation reaction, as indicated by the following formulae:[202]

$$CeO_{2(surface)} + M^+ \leftrightarrow CeO_2 \cdot M^+_{(surface)} \quad (9)$$

$$CeO_2 + M^+ + e^- \leftrightarrow CeO \cdot OM \quad (10)$$

where M represents a cation such as H^+, Na^+, or K^+. The first process is the non-Faraday reaction, which is the straightforward adsorption or desorption of M^+ on the surface of CeO_2. The second is the Faraday process, in which M^+ is intercalated or de-intercalated into or from CeO_2, changing the valence of Ce from IV to III. The electrolyte's ion intercalation and deintercalation speed, as well as the electrode material's redox activity, are both essential for the pseudocapacitive performance, as we may infer from the reaction mechanism. In light of the above factors, researchers have improved the efficiency of CeO_2 electrode materials for storing energy by: I. preparing nanoparticles, II. controlling the morphology, III. engineering the pores, IV. introducing defects and ions, V. exposing highly active surfaces, VI. doping with highly conductive materials, *etc.*

Nanostructured CeO_2 is a significant application-relevant electrode material. The specific surface area and particle morphology are crucial elements that influence pseudocapacitive performance. The further development direction of nanoparticles is to use a large specific surface area and special morphology to achieve optimum pseudocapacitive dynamic performance and optimize the theoretical specific capacity. In order to investigate high-performance CeO_2 electrode materials, Wang *et al.* using propylene oxide as a precipitant, prepared spherical and linear CeO_2 nanoparticles in aqueous and ethanolic solutions, respectively.[203] The acidity of the cation in the solution affects how propylene oxide reacts. Since Ce^{3+} has greater acidity in ethanol solution, it can rapidly produce CeO_2. CeO_2 was orientated on the high surface energy {110} plane to grow and link, resulting in wire-like crystals. In an aqueous solution, its growth process follows an isotropic growth

Table 5 Research results of CeO_2 as a pseudocapacitive electrode material

Materials	Synthesis method	Electrolyte	Potential (V)	Capacitance (F g^{-1})	Capacitance retention (%)	Reference
Hexagonal CeO_2 nanoparticles	Hydrothermal method	1 M NaCl	0–0.8	457.0 (2 A g^{-1})	82.0 (2000 cycles)	202
CeO_2–W nanocrystals	Epoxide precipitation reaction	3 M KOH	0–0.5	372.6 (6.3 A g^{-1})	91.0 (4000 cycles)	203
CeO_2 nanocrystal	Supercritical hydrothermal method	6 M KOH	0–0.4	339.5 (1 A g^{-1})	85.7 (1000 cycles)	204
CeO_2 mesoporous microsphere	Assisted microwave method	3 M KOH	0–0.45	773.0 (5 mV s^{-1})	56.3 (3000 cycles)	205
CeO_2 nanostructures	Combustion method	1 M KOH	−0.3–0.45	114.6 (10 mV s^{-1})	92.5 (1000 cycles)	206
CeO_2@20 nanoparticles	One step solvothermal method	1 M Na_2SO_4	0–0.8	143.0 (0.2 mA g^{-1})	75.0 (1000 cycles)	207
CeO_2 nanoparticles	Precipitation and the hydrothermal method	1 M LiCl	−0.8–0.8	877.5 (3 A g^{-1})	96.5 (5000 cycles)	208
Hexagonal CeO_2	Hydrothermal method	1 M HCl	0–0.8	889.0 (2 mV s^{-1})	~100 (1500 cycles)	209

mechanism, thus forming spherical crystals. Electrochemical tests reveal that CeO_2 nanospheres have better pseudocapacitive properties than CeO_2 nanowires. To investigate the effect of surfactants on the morphology, size, and exposed crystal faces of CeO_2 nanocrystals in greater depth, Hao *et al.* synthesized CeO_2 nanocrystals using supercritical hydrothermal synthesis.[204] The results indicate that cubic CeO_2 has a greater pseudocapacitive performance because of the highly active {100} plane on the exposed surface and the nanoparticle size. This study elucidates the crystal plane evolution and self-assembly mechanism of CeO_2, introducing a fresh concept for the construction of high-performance novel CeO_2.

In addition, controlling the morphology of nano-functional materials is one of the most effective strategies for enhancing their performance. Cheng *et al.* achieved high-efficiency energy storage by effectively controlling the morphology of CeO_2 nanoparticles.[205] They synthesized CeO_2 mesoporous nanospheres using a simple microwave process and sodium citrate as a chelating agent. As sodium citrate formed citric acid during hydrolysis and created alkaline conditions, it was economical because no urea was required. After 3000 cycles at 0.1 mA cm^{-2}, the as-prepared CeO_2 still exhibits a high specific capacitance of 415 F g^{-1}, an exceptional lithium storage capacity of 529 mA h g^{-1} after 100 cycles at 0.5 mA g^{-1}. CeO_2's superior electrochemical performance is due to its unique mesoporous microsphere structure. On the basis of this research, Abdul Jabbar Khan *et al.* synthesized porous CeO_2 nanoparticles as electrode materials and used highly conductive carbon cloth as a current collector.[206] CeO_2 nanoparticles supported on carbon cloth exhibit excellent energy storage performance, with a specific capacitance of 877.5 F g^{-1} at 3 A g^{-1} and capacity retention of 96.52% after 5000 cycles. This further demonstrates the critical role of a porous structure in enhancing CeO_2 pseudocapacitive performance. On the basis of the aforementioned research findings, Nallappan Maheswari and Gopalan Muralidharan developed ultra-high-performance CeO_2 electrode materials, which represented a significant milestone in the development of CeO_2 electrode materials.[207] They prepared hexagonal nanostructured CeO_2 by a one-step hydrothermal method using cetyltrimethylammonium bromide (CTAB) as a surfactant; the formation mechanism is shown in Fig. 13a. They maintained the reaction environment's pH at 10. The OH^- content is saturated under these conditions, and CTAB ionizes CTA^+ and regulates the rate at which NaOH ionizes OH^-, resulting in the formation of well-defined hexagonal CeO_2. In this work, the effects of different calcination temperatures on the shape, structure, and electrochemical performance of CeO_2 were looked at in greater detail. CeO_2 calcined at 500 °C, named C-500, has the greatest active surface area and porosity, which promotes the rapid diffusion of electrolyte ions and has fast kinetics, resulting in the best electrochemical performance. When the charge–discharge current density was increased from 2 to 10 A g^{-1}, the specific capacity declined from 927 to 475 F g^{-1} at a retention rate of 51.24% (Fig. 13b). After 1500 cycles at a high current density of 20 A g^{-1}, the capacity can still be maintained at over 100%, as shown in Fig. 13c. Additionally, an asymmetric supercapacitor utilizing activated carbon as the anode was fabricated. The device had a high energy density of 45.6 W h kg^{-1} at a power density of 187.5 W kg^{-1} with good cycle stability (Fig. 13d). The pseudocapacitive properties of hexagonal CeO_2 nanoparticles were further investigated in aqueous solutions of NaCl, KCl, Na_2SO_4, and K_2SO_4, the four most common neutral electrolytes.[202] At a current density of 2 A g^{-1}, the specific capacitances in the four electrolytes were 457, 395, 400, and 320 F g^{-1}, respectively. This is because Na^+ has a lower radius than K^+, and SO_4^{2-} has a substantially higher ionic radius than Cl^-. When the hydration radius is similar, ions with a smaller radius spread more rapidly. This shows the crucial function of selecting an appropriate electrolyte for improving the pseudocapacitive performance of CeO_2 electrode materials.

Finally, researchers investigated the mechanism by which oxygen vacancies affect the electrochemical performance. Prasanna and his team synthesized ultra-porous CeO_2 nanoparticles containing oxygen vacancies (CeO_2 NS) with a fast and low-cost combustion method.[208] Capacitance retention after 1000 cycles was 92.5% at 1 A g^{-1}. The resistances to charge transfer were 2.01 Ω and 2.86 Ω, respectively, before and after cycling. The CeO_2 NS exhibits outstanding kinetics and cycling stability thanks to the oxygen vacancies and porous structure. Manjeet Kumar *et al.* investigated the influence of oxygen vacancies on electrochemical performance in detail.[209] The oxygen vacancy content of CeO_2 was quantified using XPS. Experiments demonstrate that raising the concentration of Ce^{3+} in CeO_2 stimulates the formation of additional oxygen vacancies on the surface, which is essential for redox activity.

But enabling CeO_2 to have a high capacitance and be stable during cycling are still big problems that make it hard to use it as an ideal electrode material. The disparity in electrochemical performance between theory and practice is related to the low conductivity of CeO_2 (8.24×10^{-8} S cm^{-1}) and the lattice expansion that happens during the reduction of Ce^{4+} to Ce^{3+}.[210] As a result, compositing CeO_2 with conductive polymers, carbon materials and their derivatives provides another effective and convenient method of increasing pseudocapacitive energy storage ability.[211] In Table 6, the typical electrochemical parameters of CeO_2 composites are compared to those of pure CeO_2. It can be seen that CeO_2 composites have a greater specific capacitance than pure CeO_2.[212–216]

Unfortunately, carbon compounds and their derivatives are difficult to produce, costly, and difficult to process.[217,218] The cycle stability of conductive polymers is poor and harmful to the environment. Because of this, it is necessary to explore other strategies to enhance the capacitance and cycling stability of CeO_2. Despite the immaturity of current research in this field, fortunately, significant progress has been achieved in the study of the conductivity of transition metal oxides (TMO) with similar properties to CeO_2.[219] Numerous studies have demonstrated that the key to enhancing the electrical conductivity of TMO is to regulate their electronic structure, energy band structure, and reactive sites. To begin with, a Schottky heterojunction is built by tweaking the electronic structure in order to lower the amount of energy that is released while carriers are being transmitted.[220] In addition, the energy band is changed to generate a z-type heterojunction in order to boost the separation

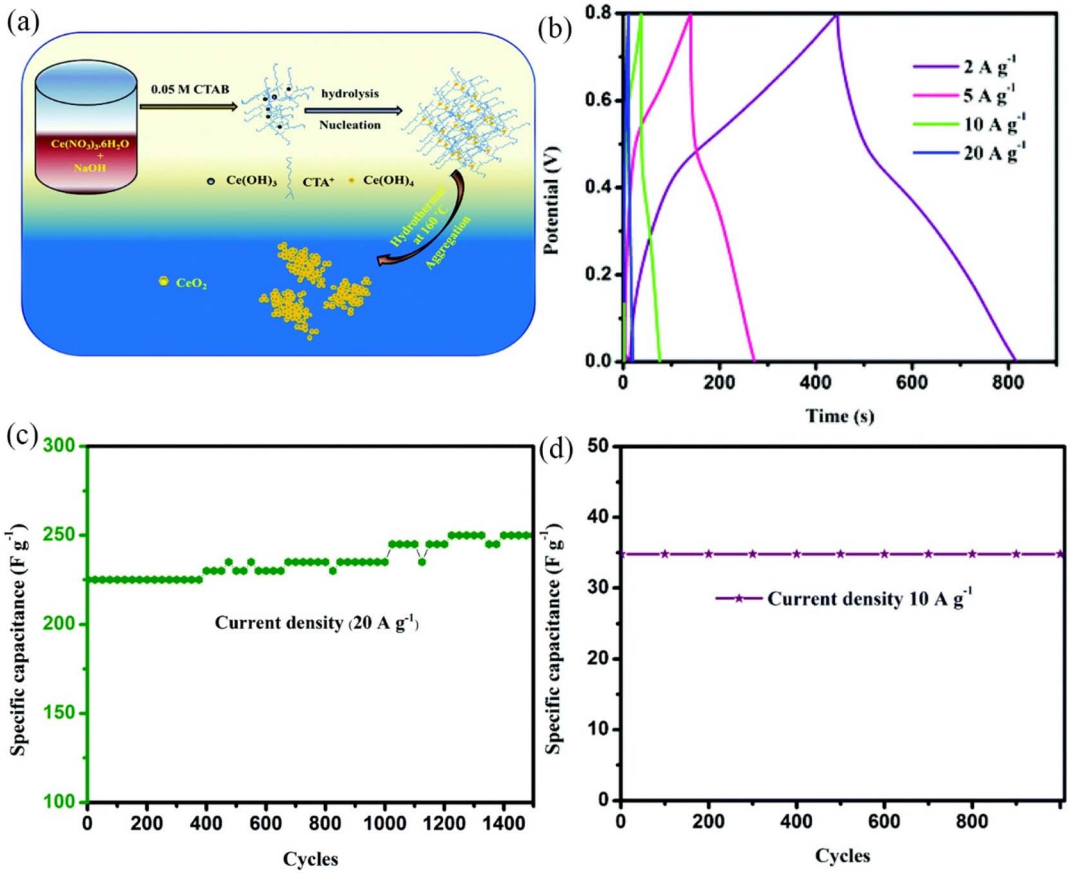

Fig. 13 Flowchart of fabrication and electrochemical characteristics: (a) schematic diagram of the formation of CeO_2 nanoparticles, (b) charge and discharge curves of CeO_2 electrodes with different current densities, (c) cycling stability of CeO_2 calcined at 500 °C electrodes, (d) cycling stability of asymmetric supercapacitor devices.

rate of hole–electron pairs.[221] In conclusion, the development of a distinct p–n junction by an internal electric field accelerates the movement of hole–electron pairs.[222] Improving electrical conductivity by promoting electron transport by doping and defect engineering is still the prevalent strategy at the present time. In addition, by modifying the electron and crystal structure, more reactive sites can be exposed, and the hole–electron pair can be split through the heterojunction, thereby promoting redox processes and providing extra charges for pseudocapacitive storage. Currently, improving electrical conductivity by promoting electron transport by doping and defect engineering is still the prevalent strategy at the present time. Furthermore, the conductivity can be enhanced by modifying the electronic and energy band structures, producing heterogeneous knots, introducing interface effects, and other strategies. The preceding investigations have significant reference value for further boosting the conductivity of CeO_2.

In addition, the effect of the electrolyte on the electrochemical performance of a CeO_2 electrode cannot be ignored. In addition to selecting an electrolyte with the most appropriate ionic radius for the material pores, it is essential to enhance the electrode/electrolyte interface interaction. The degree of electrode material immersion in the electrolyte is paramount for defining the pseudocapacitance kinetics.[195] When electrolyte ions are well immersed in the electrode material, cations can quickly and reversibly intercalate and deintercalate, and strong interfacial contacts greatly increase the ionic conductivity of the material. However, CeO_2 is not hydrophilic; therefore

Table 6 Electrochemical properties of CeO_2-carbon/polymers composites

Materials	Potential (V)	Capacitance (F g^{-1})	Capacitance retention (%)	Reference
CeO_2/CNTs	0.3–0.81	818 (1 mV s^{-1})	95.3 (5000 cycles)	212
CeO_2/GC	0–0.55	501 (1 A g^{-1})	93.0 (5000 cycles)	213
CNTs@CeO_2-HTs	0–1.55	70.7 mA h cm^{-2} (1 mA cm^{-2})	86.4 (3000 cycles)	214
PANI/rGO/CeO_2	−0.2–0.8	684 (1 A g^{-1})	92.0 (3000 cycles)	215
rGO-CeO_2/PANI	−1.4–0	454.8 (1 A g^{-1})	70.2 (10 000 cycles)	216

inadequate infiltration will result in a drop in pseudocapacitive kinetic properties in aqueous electrolytes, thus combining with hydrophilic substances is an efficient remedy. Layered silicate minerals possess exceptional wettability, a distinct interlayer environment, and a stable layered structure, making them perfect composite materials. Zhang *et al.* synthesized transition metal boride–clay composites by liquid-phase reduction and investigated the effect of the clay's structural type and microstructure on its electrochemical characteristics.[223] The composites exhibited exceptional electrochemical kinetics and cycling stability, according to electrochemical measurements. However, research in this field is still in its infancy, and the augmentation of electrochemical characteristics by clay minerals and the underlying mechanisms of action require additional investigation.

3.1.2 Lanthanum oxide. In addition, La_2O_3 is a pseudocapacitive energy storage material with broad potential applications. The charge storage mechanism of La_2O_3 is shown in eqn (11):

$$La_2O_3 + nM^+ + ne^- \leftrightarrow M_nLa_2O_3 \quad (11)$$

As early as 2016, Yadav *et al.* used a one-step hydrothermal method to grow rod-like La_2O_3 films on stainless steel substrates as electrode materials for flexible supercapacitors.[224] The film has a specific surface area of 45.39 $m^2\ g^{-1}$ and a pore size of 6.9 nm according to the BET calculation method. These films have a higher specific surface area and are comparable to those made by chemical deposition of La_2O_3, $Ni(OH)_2$, and Fe_2O_3.[225–227] Electrochemical tests were performed on rod-like La_2O_3 films, which exhibited a high specific capacity of 250 F g^{-1} and a power density of up to 1.5 kW kg^{-1} at an energy density of 80 W h kg^{-1}. A symmetric supercapacitor was assembled using PVA/$LiClO_4$ gel as the electrolyte, exhibiting a specific capacitance of 10 F g^{-1} at a scan rate of 5 mV s^{-1}, and a capacity retention of 79% after 1000 cycles. In the same year, Yadav *et al.* used one-step spray pyrolysis to fabricate cellular La_2O_3 porous films for supercapacitors and gas sensors.[228] After 3000 cycles, the La_2O_3 film retains 85% of its specific capacitance (166 F g^{-1}), indicating good cycling stability. According to the research outlined above, Wang *et al.* synthesized La_2O_3 thin films using a straightforward one-step hydrothermal method for the purpose of investigating electrowetting responses for high-performance supercapacitors.[229] The study discovered that by adjusting the hydrothermal temperature and time, the surface structure of the La_2O_3 thin film can be precisely controlled. SEM images of La_2O_3 thin films hydrothermally heated for 20 hours at various temperatures are shown in Fig. 14a–f. As the temperature is increased from 150 to 160 °C, the microspheres grown on the titanium substrate become denser. At 170 °C, the microspheres form a dense membrane structure; at 180 °C, an La_2O_3 hierarchical structure with vertically arranged flower-like nanoparticles is formed. When the temperature is increased to 190 °C, the microspheres aggregate into a dense microsphere film, indicating that 180 °C is the critical temperature for the formation of a flower-like hierarchical structure. The hydrothermal reaction time (10, 15, and 20 h) was changed at the optimal temperature of 180 °C. The morphologies of the prepared samples are shown in Fig. 15a–c. Based on the XRD patterns of samples made under different reaction conditions (shown in Fig. 15d), the hydrothermal method was able to make an La_2O_3 film with dense microspheres that look like flowers and nano-metal structures that are arranged in a hierarchical way. No effect was observed on the ingredients under different reaction conditions. The CV curves clearly illustrate the pseudocapacitive features of the samples (Fig. 15e), and the specific capacitance changes with hydrothermal temperature, as illustrated in Fig. 15f, indicating that the prepared La_2O_3 film has a high specific capacitance and that hydrothermal temperature has a significant effect on its capacitance. Additionally, Yadav *et al.* investigated the practicality of La_2O_3.[230] Chemical water bath deposition was used to fabricate Co_3O_4 and La_2O_3 thin films. In 1 mol L^{-1} KOH, the specific capacitances are 415 F g^{-1} and 288 F g^{-1}, respectively. A highly conductive oxide film of Co_3O_4 was used as the anode, an La_2O_3 film was used as the cathode, and PVA-KOH gel was used as the solid electrolyte. The device has a high specific capacitance of 15 F g^{-1} and retains 92% of its high cycling performance after 2000 cycles. When the power density is 108.2 W kg^{-1}, the energy density is as high as 42.9 W h kg^{-1}. When two asymmetric capacitors are connected in series, the LED can remain illuminated for 45 seconds after being fully charged.

Graphene and its derivatives (r-GO) have emerged as star materials in the field of supercapacitor energy storage in recent years due to their large specific surface area, high conductivity, high electron mobility, and chemical stability.[231] As a result, composites of La_2O_3@G(r-GO) have a greater energy storage capacity and a more stable cycle life than pure La_2O_3. Zhang and his peers synthesized reduced graphene oxide/lanthanum oxide (r-GO/La_2O_3) nanocomposites using a straightforward and cost-effective reflow method.[232] Throughout the process of condensation reflow, graphene oxide (GO) was broken down, and La_2O_3 was successfully added to the surface of GO. Electrochemical tests were conducted in a 3 mol L^{-1} KOH electrolyte. At a current density of 0.1 A g^{-1}, the r-GO/La_2O_3 composite had a specific capacitance of 156.25 F g^{-1} and a capacity retention of 78% after 500 cycles. The composite material's superior electrochemical performance is due to the fact that the addition of La_2O_3 reduces the degree of aggregation of the graphene sheets and increases their effective active specific surface area, thereby increasing the electrode material's specific capacitance. The r-GO/La_2O_3 composites were used to assemble button cells. When the power density is increased to 15.62 kW kg^{-1}, the energy density value increases to 13.02 W h kg^{-1}, indicating the r-GO/La_2O_3 composite's suitability for practical applications. Similarly, Karthikeyan *et al.* synthesized lanthanum oxide/reduced graphene oxide (La_2O_3/r-GO) nanocomposites by a simple hydrothermal method.[233] The interfacial effect of La_2O_3 and r-GO significantly improves the specific capacitance and cycling stability of electrode materials, as demonstrated in this work. The specific capacitance of La_2O_3/r-GO is as high as 546 F g^{-1} (at 2 mA g^{-1}) in an electrochemical test using the traditional three-electrode system, and the capacity remains at 92.3% after 10 000 cycles, demonstrating extraordinary cycle stability. R-GO

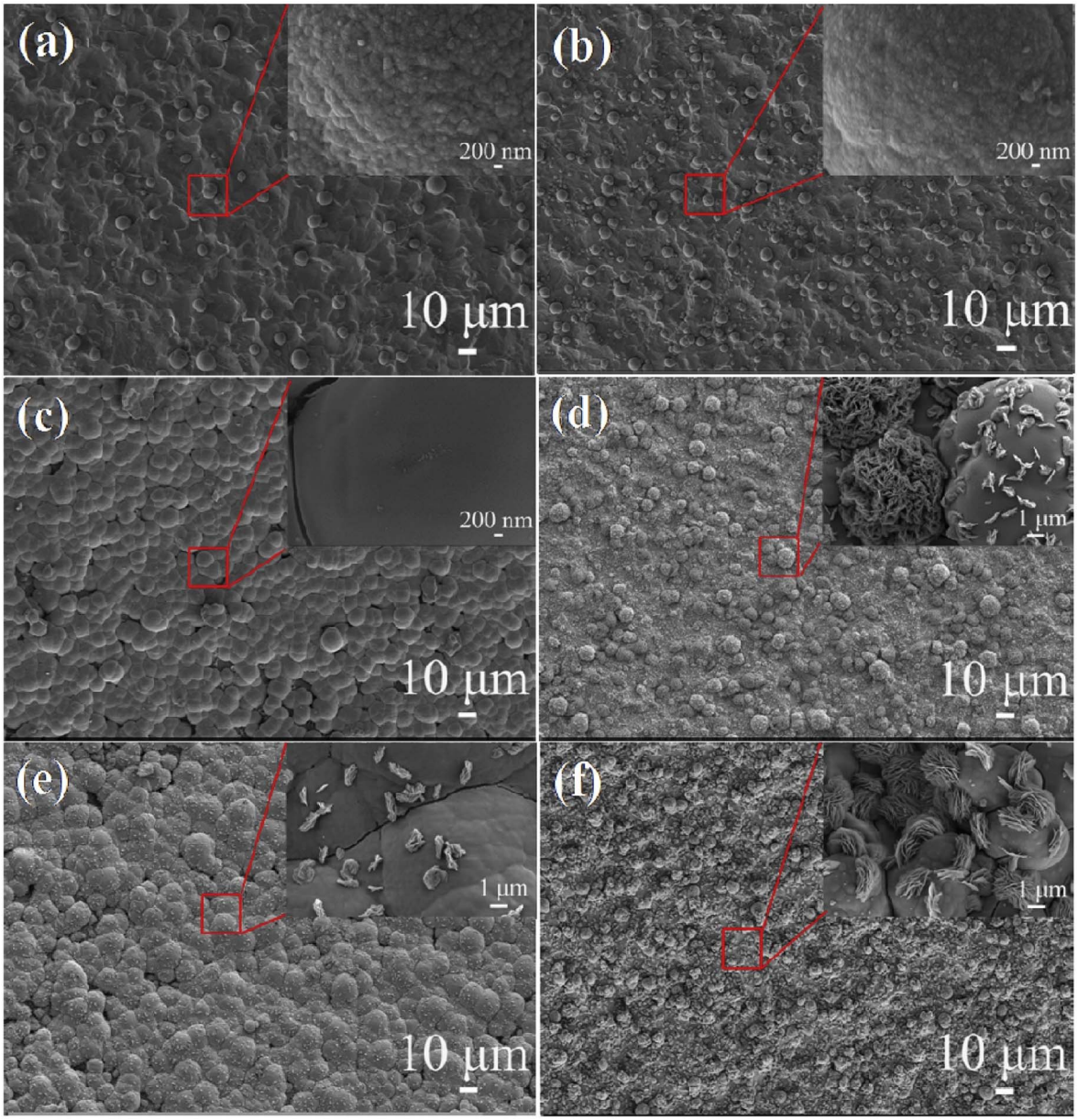

Fig. 14 SEM images of samples with different hydrothermal times: (a) 150 °C, (b) 160 °C, (c) 170 °C, (d) 180 °C, (e) 190 °C and (f) 180 °C. SEM magnified images of the inset marked areas.

increases the La_2O_3/r-GO composites' effective specific surface area, improves their electrical conductivity, and accelerates charge transport, thus enhancing the composites' redox activity. The interfacial effect of r-GO and La_2O_3 boosts electrolyte adsorption at the interface, increases the wettability of the electrode material and electrolyte, and reduces the ion transport distance, effectively improving the composites' pseudocapacitive performance. Additionally, the author proposes a cost-effective way to combine supercapacitors and clean energy. Solar energy's application value will increase even further if it can be converted to electricity *via* supercapacitors. Miah *et al.* also investigated the temperature dependency of capacitance by utilizing the interface effect between GO and La_2O_3.[234] High-performance supercapacitors degrade the active material at elevated temperatures, restricting their applicability range. As a result, it is vital to enhance supercapacitors' thermal stability. Miah prepared GO-La_2O_3 composites exhibiting 158% and 205% increases in specific capacitance at 30 °C and 70 °C, respectively, compared to pure GO. When the current density was 1 A g^{-1} and the temperature was 70 °C, the specific capacitance increased to a maximum of 751 F g^{-1}. After 2000 cycles, the electrode capacity retention rate was 78% at 30 °C and 67% even at 70 °C, indicating excellent thermal stability. The effect of temperature on the charge transport properties of La_2O_3 was investigated by examining the current–voltage characteristics of samples at temperatures ranging from 0 to 70 °C. Fig. 16(a and b) depict the *J*–*V* curve. The *J*–*V* curve is nearly symmetrical across the entire voltage range, and the current is

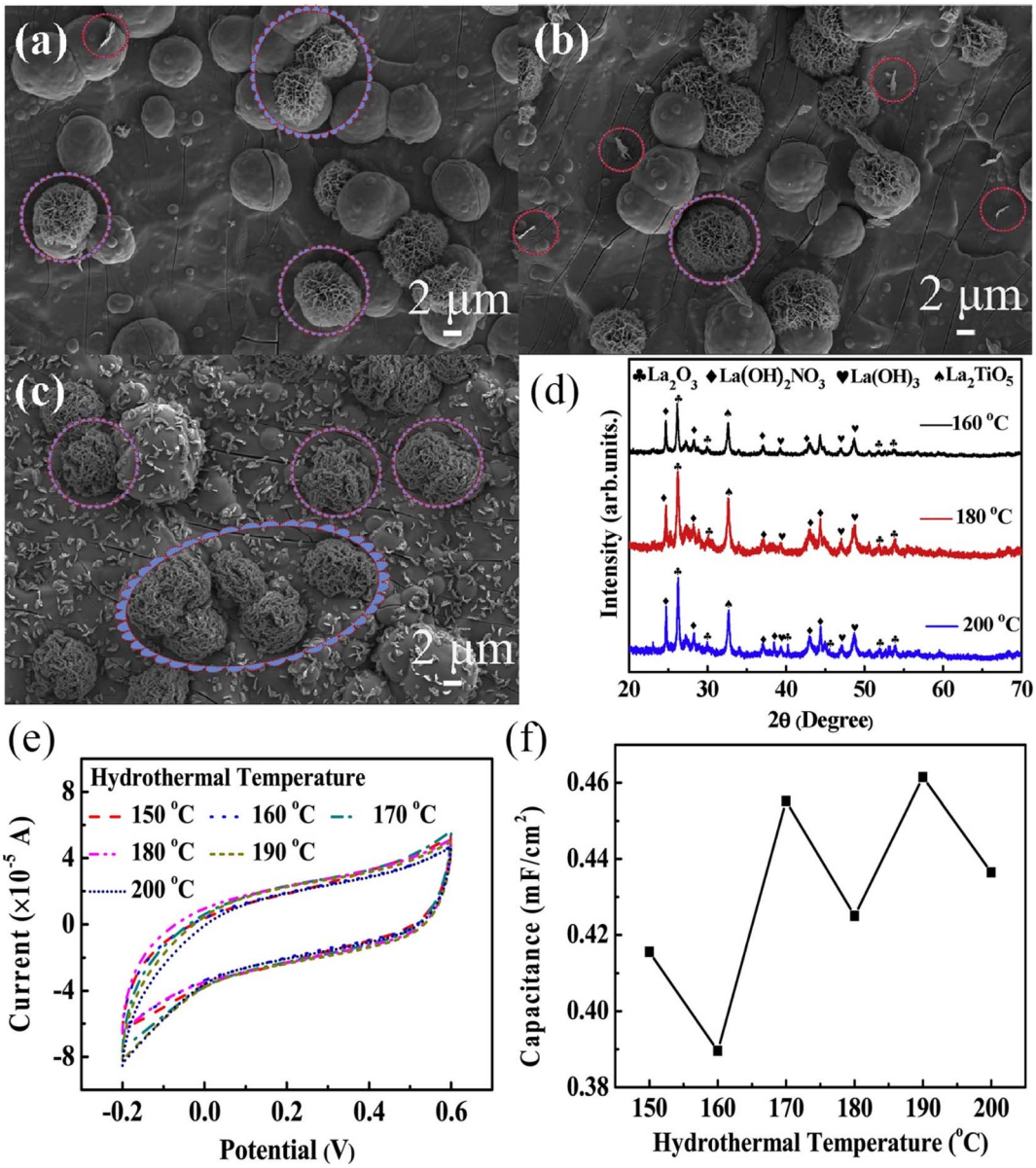

Fig. 15 SEM, XRD characterization and electrochemical properties: (a–c) the SEM images of samples under different hydrothermal times: (a) 10 h, (b) 15 h and (c) 20 h, (d) the XRD pattern of the samples at 160, 180, and 200 °C, (e) CV curves of Ti-based La_2O_3 films prepared at different hydrothermal temperatures, (f) the corresponding specific capacitance at different temperatures.

linear with the bias voltage at low voltages (±0.5 V), indicating that the conduction process is ohmic. However, as the bias high voltage increases, a nonlinear relationship emerges, with the degree of nonlinearity increasing with temperature. This is because high temperature increases the conductivity of the electrode material, and high temperature induces internal field emission, resulting in a linear deviation. Eqn (12) can be utilized to determine the voltage contribution (V^m) of the inner field emission:[235]

$$J = \sigma V + CV^m \quad (12)$$

where σ represents the linear conductivity. Table 7 lists the relevant parameters fitted by eqn (12). Fig. 16c provides a more straightforward explanation for the interface effect generated by internal field emission. Since the Fermi level of graphene is significantly higher than that of La_2O_3, charge transfer occurs at the two-phase interface at higher temperatures and the induced charge transfer increases as the temperature rises. This charge transfer mechanism increases the electrochemical response at higher temperatures, hence enhancing the pseudocapacitive performance.

Since Trasatti S studied the pseudocapacitive properties of RuO_2 and found that its theoretical specific capacitance is as high as 1300–2200 F g^{-1}, more and more studies have been devoted to transition metal compounds (TMs).[236] The highly reversible redox reaction between transition metal compounds and electrolyte ions provides ultra-high capacitance, but RuO_2

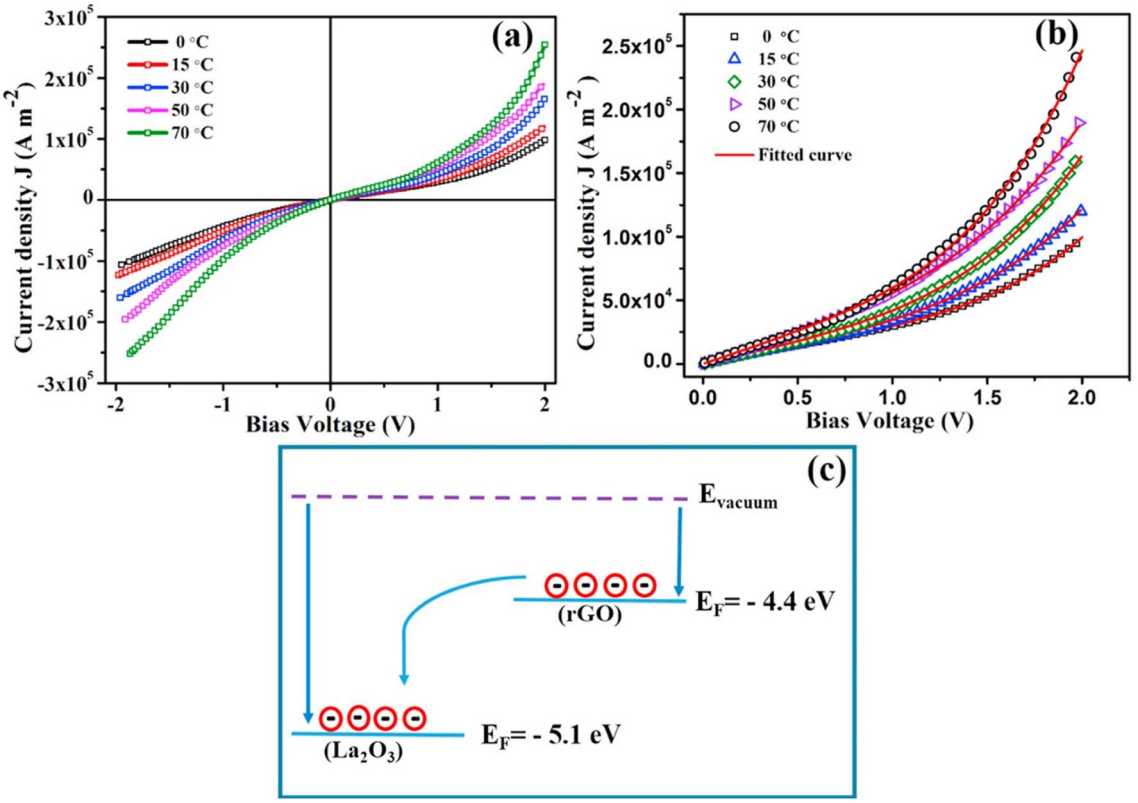

Fig. 16 *J*–*V* characteristics of G-La_2O_3 at different temperatures: (a) full-range experimental *J*–*V* plots, (b) half-range *J*–*V* fitting, (c) schematic of charge transfer from rGO to La_2O_3.

Table 7 Parameter values obtained from eqn (14) (ref. 235)

Temperature (°C)	σ (S m^{-1})	C	m
0	27 891	1778	3.10
15	29 238	5301	3.27
30	35 004	6972	3.75
50	47 969	8290	4.04
70	51 095	8743	4.61

is expensive and toxic, so Ni-based, Mn-based, and Co-based compounds have become promising pseudocapacitive electrode materials.[237] Sun *et al.* deposited MnO_2 and La_2O_3 on carbon paper as working electrodes, and assembled an asymmetric supercapacitor.[238] By effectively increasing the potential range of the working electrode, the capacitor's energy density was greatly increased, and the range of uses for the capacitor grew. In 0.5 mol L^{-1} Na_2SO_4 electrolyte, the asymmetric supercapacitor exhibits a mass energy density of 80.56 W h kg^{-1} and a volumetric energy density of 0.74 mW h cm^{-3}. After further encapsulation into a device, the power density remains at 94.29 mW cm^{-3} while the energy density is 0.49 mW h cm^{-3}. Duan *et al.* synthesized ultrathin triangular sheet $Ni(OH)_2$ and La_2O_3 composites (LONH) by a simple solvothermal method.[239] LONH exhibits excellent electrochemical energy storage performance. This study shows that the addition of La_2O_3 to transition metal compounds (TMs) can effectively change the morphology and structure of the composites, providing a new vision to develop novel La-TM electrode materials with excellent performance. Li *et al.* added La_2O_3 as an electrocatalyst to MnO_2, and prepared waxberry-shaped Mn–La composite microspheres by a two-step hydrothermal method.[240] The lattice defects and electrocatalytic functions of La_2O_3, which improve the active specific surface area of the electrode material and speed up the rate of charge transfer, give the composite its excellent rate performance and ultra-high cycle stability.

3.1.3 Other RE_2O_3. Other RE_2O_3 also offer potential for pseudocapacitive energy storage, such as Nd_2O_3, Sm_2O_3, Eu_2O_3, and Gd_2O_3.[241] However, due to the poor electrochemical stability and relatively low energy storage efficiency of the above pure rare earth oxides, most research has concentrated on compounding with carbon materials, metal compounds, and conductive polymers. The charge storage mechanism of RE_2O_3 is shown in eqn (13) and (14):

$$RE_2O_3 + nM^+ + ne^- \leftrightarrow M_nRE_2O_3 \quad (13)$$

$$2RE(OH)_2 + 2OH^- \leftrightarrow RE_2O_3 + 2e^- + 3H_2O \quad (14)$$

Mohammad Shiri *et al.* fabricated Nd_2O_3 nanorod composite conductive polymer films by ultrasonic-assisted pulsed electrochemical deposition, which exhibited significantly higher rate capability and superior cycling stability than conductive

polymer films.[242] Liu *et al.* prepared polypyrrole/Sm_2O_3 (PPy/Sm_2O_3) nanocomposites by *in situ* chemical oxidative polymerization, and the half-cell exhibited a large capacitance of 771 F g^{-1} in 1 M $NaNO_3$.[243] This demonstrates that Sm_2O_3 is an energy storage material with potential electrochemical applications. Similarly, Shiri and his research team prepared polyaniline-derivative/Sm_2O_3 (POAP/Sm) composite films by electrochemical deposition.[244] The electrode material exhibits excellent cycling stability, with a capacity retention of 91% and a coulombic efficiency of 95% after 1000 cycles. Further, Mohammadian-Sarcheshmeh *et al.* prepared *p*-phenylenediamine/Sm_2O_3 (PPDA/Sm_2O_3) cross-linked graphene oxide (GO) aerogels by a simple hydrothermal method.[245] Through the nucleophilic addition reaction of amino groups on PPDA and carboxy groups on GO, the stacking of graphene oxide layers can be stopped, and the space between graphene oxide layers can be altered to greatly improve the composite's electrochemical performance. This porous three-dimensional PPDA/Sm_2O_3 cross-linked GO aerogel structure greatly improves the specific capacity of the electrode material, and the specific capacitance is as high as 591 F g^{-1} at a scan rate of 5 mV s^{-1}, which is about nine times higher than that of pure Sm_2O_3, and it has good cycle stability, with a capacity retention of 92.7% after 4000 cycles. The porous three-dimensional structure proposed in this study can be extended to other electrode material designs, which is beneficial to improving the electrochemical kinetics and greatly improving the energy storage efficiency of pseudocapacitors. On this basis, Shiri *et al.* prepared POAP/Eu_2O_3 and POAP/Gd_2O_3 by the pulsed electrochemical deposition method.[246,247] The enhanced electrochemical performance of the composites is due to the special surface structure as well as the synergistic effect of the two components.

3.1.4 Other rare earth oxides. Praseodymium oxide is a special rare earth oxide. Praseodymium oxide has various stoichiometric oxides, such as Pr_2O_3, PrO_2, Pr_4O_7, and Pr_6O_{11}, among which Pr_6O_{11} is a phase that exists stably at ambient temperature. Pr_6O_{11} has excellent oxygen mobility and redox activity, and rapid ionic transitions between mixed valence states in the Pr_6O_{11}, resulting in high conductivity (σ = 7.6 μS cm^{-1}); consequently it has been employed for electrochemical energy storage.[248] The charge storage mechanism of Pr_6O_{11} is shown in eqn (15) and (16):

$$Pr_6O_{11} + nM^+ + ne^- \leftrightarrow M_nPr_6O_{11} \quad (15)$$

$$6Pr(OH)_2 + 10OH^- \leftrightarrow Pr_6O_{11} + 6e^- + 11H_2O \quad (16)$$

As early as 2011, Wang *et al.* prepared Pr_6O_{11}/polypyrrole (Pr_6O_{11}/PPy) with a core–shell structure, whose specific capacitance can reach 400 F g^{-1} at a current density of 10 mA cm^{-2}.[249] Similarly, Kubra *et al.* presented Pr_6O_{11}/Mn_3O_4 composites by a simple hydrothermal method, exhibiting a high 794.58 F g^{-1} ratio capacitance at 0.5 A g^{-1} current densities.[250] Based on the research cited above, Chen *et al.* prepared a Pr_6O_{11}–$NiCo_2O_4$ core–shell structure with better performance, coating Pr_6O_{11} as a growth framework on nickel foam (NF), and Pr_6O_{11}–$NiCo_2O_4$ exhibited an ultra-high specific capacitance of 1635 F g^{-1} at 0.5 mA cm^{-2}.[251] Paravannoor *et al.* prepared PrO_x/unzipped multi-walled carbon nanotubes (PrO_x/UZCNT) and presented the unique insight that the anion intercalation effect generated by surface oxygen vacancies enhances the electrochemical performance.[252] Fig. 17a lists the work functions of different metal oxides. The assembly of low-work-function Pr_6O_{11} (2.8 eV) with high-work-function compounds (V_2O_5, 6.85 eV) can prepare supercapacitors with a wide potential window exceeding 4 V, thereby significantly improving the energy density of the supercapacitor. The value is calculated from eqn (17) and (18):[252]

$$E = E_0 + E_1 + E_2 \quad (17)$$

$$E_0 = \left(\omega^{\beta} + \omega^{\alpha}\right)\frac{N_a}{F} \quad (18)$$

where ω^{β} and ω^{α} represent the work function, ΔE_1 and ΔE_2 represent the electrode potential, and N_a is the Avogadro number. Through conventional morphology and structure methods, such as XRD, SEM, and TEM (Fig. 17b–f), it is proved that the method proposed by Anjali successfully prepared oxygen-vacancy-rich rod-like PrO_x/UZCNT. The grain growth is controlled by a simple solid–liquid reaction during the hydrothermal process: $Pr(OH)_3$ grows one-dimensionally on the surface of carbon nanotubes, Pr_6O_{11} is obtained by calcination, and the remaining NO_3^- and K^+ are embedded in the nanotubes. The unzipped carbon nanotubes are formed without destroying the interface structure between Pr_6O_{11} and carbon. Fig. 17g clearly illustrates the above-mentioned formation mechanism. Electrochemical tests on the as-prepared PrO_x/UZCNT and PrO_x (Fig. 18a) show that PrO_x/UZCNT exhibits better pseudocapacitive performance, which is attributed to the oxygen vacancies in PrO_x/UZCNT. Fig. 18c is a schematic representation of the method through which oxygen vacancies in PrO_x/UZCNT contribute to electrochemical energy storage. Anion vacancies accelerate the diffusion of oxygen in the unit cell and promote the interconversion of Pr^{3+} and Pr^{4+}. By comparing the peaks of O 1s orbitals of the samples before and after the cycle by an XPS test (Fig. 18b(1 and 2)), it was discovered that the quantity of oxygen vacancies decreased, indicating that oxygen vacancies contribute to the redox process. Finally, an asymmetric supercapacitor was assembled using PrO_x/UZCNT with a small work function and V_2O_5-graphene with a large work function, with a potential window as high as 3.8 V. When the power density is 2.9 kW kg^{-1}, the energy density is as high as 52.08 kW h kg^{-1}, and the capacity retention rate is ≥ 95% after 2000 cycles (Fig. 18d–f). This study provides an effective strategy for extending the potential range of electrode materials to fabricate a high-energy-density supercapacitor.

The above research on the pseudocapacitive properties of rare earth oxides opens up new horizons for the future development of high-performance nanocomposites.

4 Conclusion and outlook

This article has described the applications of rare earths in traditional metallurgy, biomedicine, magnetism, luminescence,

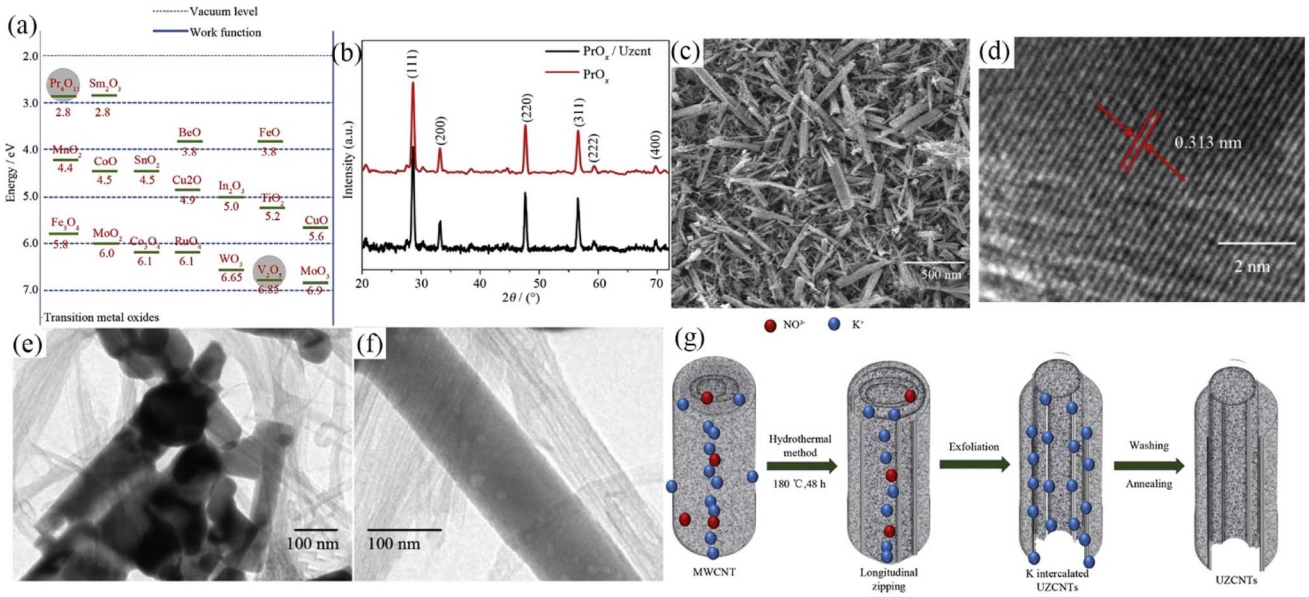

Fig. 17 Summary of oxide work functions and structural characterization of samples: (a) summary of the work functions of different oxides, (b) XRD of PrO_x and PrO_x/U_{zcet} samples, (c) SEM images of PrO_x/U_{zcet}, (d) HR-TEM images of PrO_x/U_{zcet}, (e and f) TEM images of PrO_x/U_{zcet}, (g) schematic illustration of the formation of zipping carbon nanotubes.

catalysis, and the energy storage field. In recent years, the rare earth industry's new development model has been based on the economics of sustainable development, clean production, and industrial ecology, shifting from traditional high energy consumption, resource waste, and environmental pollution to green ecological development, which is a green resource that can be utilized in new energy storage fields. On the basis of the electrochemical energy storage potential of rare earths, typical

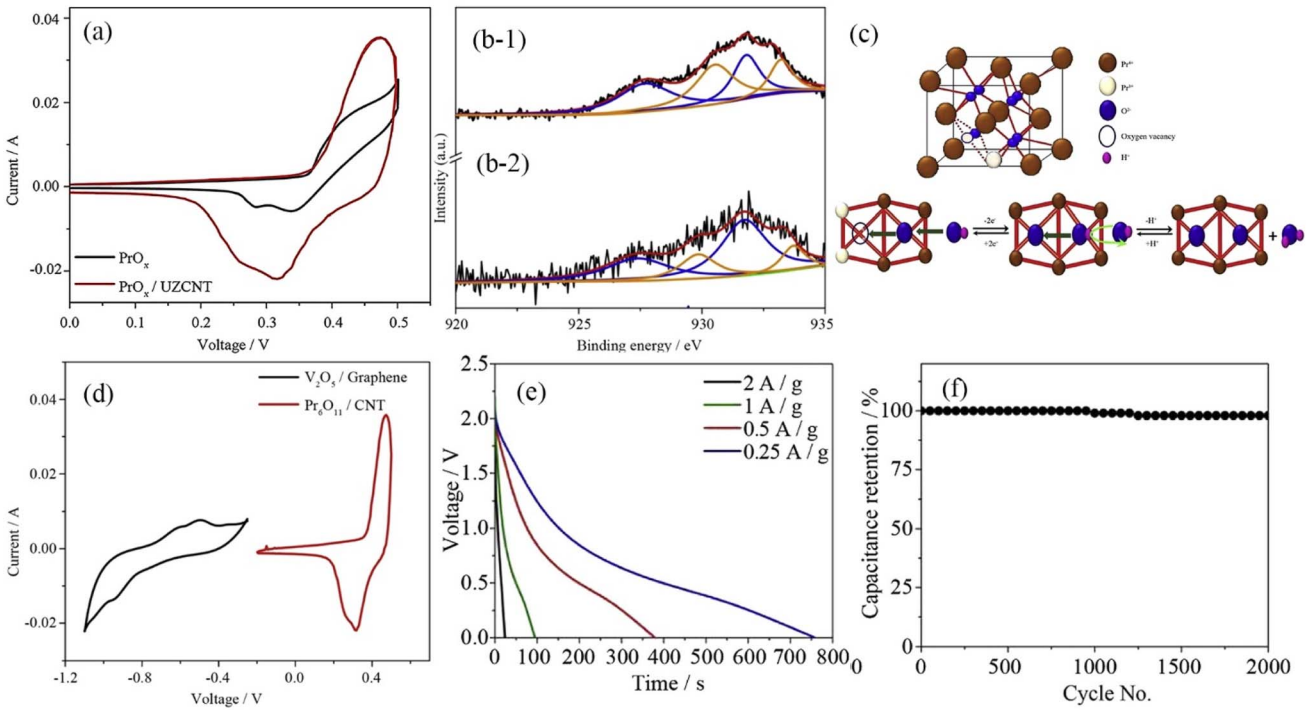

Fig. 18 XPS and electrochemical properties of PrO_x and PrO_x/U_{zcet}: (a) CV curves of PrO_x and PrO_x/U_{zcet} at 50 mV s^{-1}, (b-1) XPS spectra of the Pr 3d state before charging, (b-2) XPS spectra of the Pr 3d state after charging, (c) formation mechanism of oxygen vacancies, (d) CV curves of Pr_6O_{11}/CNT and V_2O_5/graphene at 50 mV s^{-1}, (e) the charge–discharge curve of the asymmetric capacitor after 2000 cycles, (f) cyclic stability of the asymmetric capacitor.

rare earth oxides were selected as research objects to provide a comprehensive overview of their research progress in the field of pseudocapacitors, including energy storage mechanisms, electrochemical performance, and application prospects. As pseudocapacitive electrode materials, rare earth oxides have the following advantages: I. they are simple to prepare, have abundant resources, and are environmentally friendly. II. Excellent redox properties are possessed by RE^{3+}/RE^{2+} or RE^{4+}/RE^{3+} couples of rare earth oxides. III. Oxygen vacancies exist in the lattice of rare earth oxides, which serve as effective reactive sites. IV. They show acid and alkaline corrosion resistance, compatible with a variety of electrolytes. V. They have high volume energy density, suitable for use in small mobile devices.

However, the low conductivity and lattice expansion of rare earth oxides restrict their development as ideal electrode materials. Based on current research results, we highlight the following concerns and challenges rare earth oxides will encounter in the future energy storage field:

I. Improve conductivity. Currently, combining with highly conductive materials is an effective method for improving electrical conductivity (such as conductive polymers, carbon materials and their derivatives). However, carbon compounds and their derivatives are difficult to produce, costly, and difficult to process. The cycle stability of conductive polymers is poor and harmful to the environment. As a result, it is necessary to explore other strategies to enhance the conductivity of rare earth oxides, such as atomic and vacancy doping; heterojunction engineering; exposing active crystal planes; and introducing interfacial effects.

II. Optimize structure. The future development path of efficient RE-oxide-based pseudocapacitive materials will be to pursue stable structures, such as ultra-high-porosity structures, core–shell structures, and layered structures. In energy storage research involving transition metal oxides, several existing research designs have been modified into a core–shell structured composite that efficiently tackles the issues of volume expansion and poor electrical conductivity while elucidating the mechanism of improved electrochemical performance through first-principles and kinetic analysis. Through structural optimization, this kind of work gives a theoretical basis for and technical help in making rare earth oxide electrode materials that work better.

III. Strengthened electrode/electrolyte interface interaction. The hydrophilicity of the electrode material and electrolyte is the key point for pseudocapacitive dynamics. The adequate wetting of the electrode material by electrolyte ions is conducive to the rapid and reversible intercalation/deintercalation of cations, and high interfacial interaction substantially enhances the ionic conductivity. However, rare earth oxides are not hydrophilic, so inadequate infiltration will result in a drop in pseudocapacitive kinetic properties in aqueous electrolytes, thus combining with hydrophilic substances is an efficient remedy. Layered silicate minerals possess exceptional wettability, a distinct interlayer environment, and a stable layered structure, making them perfect composite materials. However, research in this area is still in its infancy, and the improvement in electrochemical performance and the mechanism of action of clay minerals remain obscure.

IV. Enhance comprehension of the energy storage mechanism. Despite the fact that a generally consistent understanding of the energy storage mechanism of rare earth oxides has been attained, there are still shortcomings. In particular, additional research is required to explore the mechanism by which the physical and chemical properties of electrolyte cations affect electrochemical performance and to identify whether electrolyte anions contribute to pseudocapacitance. Existing research has demonstrated that the energy storage mechanism of transition metal nitrides in KOH electrolyte is the synergistic effect of K^+ intercalation and OH^- surface electrochemical adsorption, but whether RE oxides exhibit a similar mechanism has not yet been concluded.

We believe that this review will help researchers realize the potential of rare earth compounds in pseudocapacitive energy storage and build on prior research to develop a fundamental insight into the role of rare earth compounds in pseudocapacitive energy storage. Finally, it is hoped that this article will provide readers with more effective preparation strategies and future directions for the development of rare earth compound pseudocapacitive electrode materials. Even though there are still some problems with the current study, we think that through more research, rare earth compounds will soon have better pseudocapacitive properties and more uses.

Conflicts of interest

There are no conflicts to declare.

Acknowledgements

This work was financially supported by the Science and Technology Project of Sichuan province (No. 2020YJ0163).

References

1 M. T. Costa Campi, P. del Rio and E. Trujillo-Baute, Trade-offs in energy and environmental policy, *Energy Policy*, 2017, **104**, 415.
2 F. S. Chien, How renewable energy and non-renewable energy affect environmental excellence in N-11 economies?, *Renewable Energy*, 2022, **196**, 526.
3 M. Hu, Balance between energy conservation and environmental impact: life-cycle energy analysis and life-cycle environmental impact analysis, *Energy Build.*, 2017, **140**, 131.
4 I. Yildiz, E. Acikkalp, H. Caliskan and K. Mori, Environmental pollution cost analyses of biodiesel and diesel fuels for a diesel engine, *J. Environ. Manage.*, 2019, **243**, 218.
5 V. Dusastre and L. Martiradonna, Materials for sustainable energy, *Nat. Mater.*, 2016, **16**, 15.
6 L. G. Kong, L. Y. Li, G. W. Cai, C. Liu, P. Ma, Y. D. Bian and T. Ma, Techno-economic analysis of hydrogen energy for

renewable energy power smoothing, *Int. J. Hydrogen Energy*, 2021, **46**, 2847.
7 X. Zhou, W. B. Zhang, X. Han, S. Chai, S. Guo, X. Zhang, L. Zhang, X. Bao, Y. Guo and X. Ma, Principles and Materials of Mixing Entropy Battery and Capacitor for Future Harvesting Salinity Gradient Energy, *ACS Appl. Energy Mater.*, 2022, **5**, 3979.
8 M. D. Scovell, Explaining hydrogen energy technology acceptance: a critical review, *Int. J. Hydrogen Energy*, 2022, **47**, 10441.
9 A. G. Olabi, Energy quadrilemma and the future of renewable energy, *Energy*, 2016, **108**, 1.
10 A. G. Olabi and M. A. Abdelkareem, Renewable energy and climate change, *Renewable Sustainable Energy Rev.*, 2022, **158**, 112111.
11 J. R. Miller, Perspective on electrochemical capacitor energy storage, *Appl. Surf. Sci.*, 2018, **460**, 3.
12 A. Cresce and K. Xu, Aqueous lithium-ion batteries, *Carbon Energy*, 2021, **3**, 721.
13 J. Libich, J. Máca, J. Vondrák, O. Čech and M. Sedlaříková, Supercapacitors: properties and applications, *J. Energy Storage*, 2018, **17**, 224.
14 S. S. Chai, L. Zhang, W. B. Zhang, X. Bao, Y. W. Guo, X. W. Han and X. J. Ma, Acid etching halloysite loaded cobalt boride material for supercapacitor electrode application, *Appl. Clay Sci.*, 2022, **218**, 106426.
15 X. L. Zhang, W. B. Zhang, X. W. Han, L. Zhang, X. Bao, Y. W. Guo, S. S. Chai, S. B. Guo, X. Zhou and X. J. Ma, Review-Pseudocapacitive Energy Storage Materials from Hägg-Phase Compounds to High-Entropy Ceramics, *J. Electrochem. Soc.*, 2021, **168**, 120521.
16 Poonam, K. Sharma, A. Arora and S. K. Tripathi, Review of supercapacitors: materials and devices, *J. Energy Storage*, 2019, **21**, 801.
17 X. P. Luo, Y. B. Zhang, H. P. Zhou, K. Z. He, C. G. Luo, Z. S. Liu and X. K. Tang, Review on the Development and Utilization of Ionic Rare Earth Ore, *Minerals*, 2022, **12**, 554.
18 T. Kegl, A. Kosak, A. Lobnik, Z. Novak, A. K. Kralj and I. Ban, Adsorption of rare earth metals from wastewater by nanomaterials: a review, *J. Hazard. Mater.*, 2020, **386**, 121632.
19 G. Lin, Q. L. Pan, W. Y. Wang, B. Liu, Z. Q. Huang, S. Q. Xiang, Y. R. Liu, Y. Q. Sun and J. Ye, The role of trace Sc and Y in the corrosion resistance of cold drawn Al-0.2Ce based alloys with high electrical conductivity, *J. Alloys Compd.*, 2021, **882**, 160708.
20 P. Tozman, H. Sepehri Amin and K. Hono, Prospects for the development of $SmFe_{12}$-based permanent magnets with a $ThMn_{12}$-type phase, *Scr. Mater.*, 2021, **194**, 113686.
21 Q. G. Huang, H. Lin, B. Wang, S. S. Lin, P. F. Wang, P. Sui, J. Xu, Y. Cheng and Y. S. Wang, Patterned glass ceramic design for high-brightness high-color-quality laser-driven lightings, *J. Adv. Ceram.*, 2022, **11**, 862.
22 L. Zhang, Q. Li, Y. C. Qin, X. T. Zhang, X. H. Gao and L. J. Song, Investigation on the mechanism of adsorption and desorption behavior in cerium ions modified Y-type zeolite and improved hydrocarbons conversion, *J. Rare Earths*, 2016, **34**, 1221.
23 U. R. Singh and S. Bhogilla, Performance analysis of $LaNi_5$ added with expanded natural graphite for hydrogen storage system, *Int. J. Hydrogen Energy*, 2022, **5**, 244.
24 B. Nageswara Rao, M. Venkateswarlu and N. Satyanarayana, Electrical and dielectric properties of rare earth oxides coated $LiCoO_2$ particles, *Ionics*, 2013, **20**, 175.
25 X. Y. Li, S. Hao, Z. W. Wang, C. L. Zhao and Z. B. Wang, Improving the electrical conductivity and electrochemical performance of $LiMn_2O_4$ by Sm gaseous penetration technology, *Appl. Surf. Sci.*, 2022, **599**, 153923.
26 X. Y. Li, H. M. Chen, C. Y. Yang, Y. F. Li and M. D. Wei, A new neodymium-phosphine compound for supercapacitors with long-term cycling stability, *Chem. Commun.*, 2021, **57**, 5933.
27 J. Prakash, Samriti, A. Kumar, H. L. Dai, B. C. Janegitz, V. Krishnan, H. C. Swart and S. H. Sun, Novel rare earth metal-doped one-dimensional TiO_2 nanostructures: fundamentals and multifunctional applications, *Mater. Today Sustain.*, 2021, **13**, 100026.
28 J. Liang, H. Peng, Z. M. Wang, R. Zhao, W. X. Zhang, G. F. Ma and Z. Q. Lei, Rare earth metal lanthanum–organic frameworks derived three-dimensional mesoporous interconnected carbon nanosheets for advanced energy storage, *Electrochim. Acta*, 2020, **353**, 136597.
29 M. Asadollahzadeh, R. Torkaman and M. Torab Mostaedi, Extraction and Separation of Rare Earth Elements by Adsorption Approaches: Current Status and Future Trends, *Sep. Purif. Rev.*, 2020, **50**, 417.
30 A. Akah, Application of rare earths in fluid catalytic cracking: a review, *J. Rare Earths*, 2017, **35**, 941.
31 C. L. Owens, G. R. Nash, K. Hadler, R. S. Fitzpatrick, C. G. Anderson and F. Wall, Apatite enrichment by rare earth elements: a review of the effects of surface properties, *Adv. Colloid Interface Sci.*, 2019, **265**, 14.
32 M. Traore, A. J. Gong, Y. W. Wang, L. N. Qiu, Y. Z. Bai, W. Y. Zhao, Y. Liu, Y. Chen, Y. Liu, H. L. Wu, S. L. Li and Y. Y. You, Research progress of rare earth separation methods and technologies, *J. Rare Earths*, 2022, **4**, 009.
33 Z. Y. Chen, Z. Li, J. Chen, P. Kallem, F. Banat and H. D. Qiu, Recent advances in selective separation technologies of rare earth elements: a review, *J. Environ. Chem. Eng.*, 2022, **10**, 107104.
34 J. L. Wang, M. Y. Guo, M. M. Liu and X. Q. Wei, Long-term outlook for global rare earth production, *Resour. Policy*, 2020, **65**, 101569.
35 P. E. Waudby, Rare earth additions to steel, *Int. Met. Rev.*, 1978, **23**, 74.
36 L. M. Wang and T. Du, Thermodynamics of Fe–Y–S, Fe–Y–O and Fe–Y–S–O metallic solution, *J. Less Common Met.*, 1985, **110**, 179.
37 W. L. M. Wu Yie Min and T. Du, Thermodynamics of rare earth elements in liquid iron, *J. Less Common Met.*, 1985, **110**, 187.

38 J. Y. Mao, G. Y. Chen, J. Zhao, Y. Y. He and J. B. Luo, An investigation on the tribological behaviors of steel/copper and steel/steel friction pairs *via* lubrication with a graphene additive, *Friction*, 2020, **9**, 228.
39 F. Pan, J. Zhang, H. L. Chen, Y. H. Su, C. L. Kuo, Y. H. Su, S. H. Chen, K. J. Lin, P. H. Hsieh and W. S. Hwang, Effects of Rare Earth Metals on Steel Microstructures, *Materials*, 2016, **9**, 417.
40 Y. P. Ji, M. X. Zhang and H. P. Ren, Roles of Lanthanum and Cerium in Grain Refinement of Steels during Solidification, *Metals*, 2018, **8**, 884.
41 C. Liu, Z. H. Jiang, J. B. Zhao, X. Q. Cheng, Z. Y. Liu, D. W. Zhang and X. G. Li, Influence of rare earth metals on mechanisms of localised corrosion induced by inclusions in Zr-Ti deoxidised low alloy steel, *Corros. Sci.*, 2020, **166**, 108463.
42 A. Biesiekierski, Y. C. Li and C. Wen, The Application of the Rare Earths to Magnesium and Titanium Metallurgy in Australia, *Adv. Mater.*, 2020, **32**, e1901715.
43 F. Y. Cao, Z. M. Shi, G. L. Song, M. Liu, M. S. Dargusch and A. Atrens, Influence of hot rolling on the corrosion behavior of several Mg-X alloys, *Corros. Sci.*, 2015, **90**, 176.
44 K. Gusieva, C. H. J. Davies, J. R. Scully and N. Birbilis, Corrosion of magnesium alloys: the role of alloying, *Int. Mater. Rev.*, 2014, **60**, 169.
45 O. Bouaziz, Revisited Storage and Dynamic Recovery of Dislocation Density Evolution Law: Toward a Generalized Kocks-Mecking Model of Strain-Hardening, *Adv. Eng. Mater.*, 2012, **14**, 759.
46 D. S. Gandel, M. A. Easton, M. A. Gibson and N. Birbilis, Calphad simulation of the Mg-(Mn, Zr)-Fe system and experimental comparison with as-cast alloy microstructures as relevant to impurity driven corrosion of Mg-alloys, *Mater. Chem. Phys.*, 2014, **143**, 1082.
47 Z. W. Geng, D. H. Xiao and L. Chen, Microstructure, mechanical properties, and corrosion behavior of degradable Mg–Al–Cu–Zn–Gd alloys, *J. Alloys Compd.*, 2016, **686**, 145.
48 E. D. Morales, E. Ghali, N. Hort, W. Dietzel and K. U. Kainer, Corrosion Behaviour of Magnesium Alloys with RE Additions in Sodium Chloride Solutions, *Mater. Sci. Forum*, 2003, **419**, 867.
49 N. Hort, Y. Huang, D. Fechner, M. Stormer, C. Blawert, F. Witte, C. Vogt, H. Drucker, R. Willumeit, K. U. Kainer and F. Feyerabend, Magnesium alloys as implant materials-principles of property design for Mg-RE alloys, *Acta Biomater.*, 2010, **6**, 1714.
50 K. Schlüter, Z. Shi, C. Zamponi, F. Cao, E. Quandt and A. Atrens, Corrosion performance and mechanical properties of sputter-deposited MgY and MgGd alloys, *Corros. Sci.*, 2014, **78**, 43.
51 W. Y. Wang, J. L. Zhu, N. N. Qin, Y. F. Zhang, S. Y. Li, Z. Xiao, Q. Lei and Z. Li, Effects of minor rare earths on the microstructure and properties of Cu–Cr–Zr alloy, *J. Alloys Compd.*, 2020, **847**, 155762.
52 M. F. Wang, D. H. Xiao, P. F. Zhou, W. S. Liu, Y. Z. Ma and B. R. Sun, Effects of rare earth yttrium on microstructure and properties of Mg Al Zn alloy, *J. Alloys Compd.*, 2018, **742**, 232.
53 H. F. Li, P. Y. Wang, G. C. Lin and J. Y. Huang, The role of rare earth elements in biodegradable metals: a review, *Acta Biomater.*, 2021, **129**, 33.
54 H. S. Brar, J. P. Ball, I. S. Berglund, J. B. Allen and M. V. Manuel, A study of a biodegradable Mg–3Sc–3Y alloy and the effect of self-passivation on the *in vitro* degradation, *Acta Biomater.*, 2013, **9**, 5331.
55 E. Aghion, G. Levy and S. Ovadia, *In vivo* behavior of biodegradable Mg–Nd–Y–Zr–Ca alloy, *J. Mater. Sci.: Mater. Med.*, 2012, **23**, 805.
56 X. Z. Song, L. Chang, J. Wang, S. J. Zhu, L. G. Wang, K. Feng, Y. G. Luo and S. K. Guan, Investigation on the *in vitro* cytocompatibility of Mg–Zn–Y–Nd–Zr alloys as degradable orthopaedic implant materials, *J. Mater. Sci.: Mater. Med.*, 2018, **29**, 44.
57 A. Drynda, N. Deinet, N. Braun and M. Peuster, Rare earth metals used in biodegradable magnesium-based stents do not interfere with proliferation of smooth muscle cells but do induce the upregulation of inflammatory genes, *J. Biomed. Mater. Res., Part A*, 2009, **91**, 360.
58 N. Zhao, N. Watson, Z. G. Xu, Y. J. Chen, J. Waterman, J. Sankar and D. H. Zhu, *In vitro* biocompatibility and endothelialization of novel magnesium-rare Earth alloys for improved stent applications, *PLoS One*, 2014, **9**, e98674.
59 A. Myrissa, S. Braeuer, E. Martinelli, R. Willumeit-Romer, W. Goessler and A. M. Weinberg, Gadolinium accumulation in organs of Sprague-Dawley(R) rats after implantation of a biodegradable magnesium-gadolinium alloy, *Acta Biomater.*, 2017, **48**, 521.
60 F. Feyerabend, J. Fischer, J. Holtz, F. Witte, R. Willumeit, H. Drucker, C. Vogt and N. Hort, Evaluation of short-term effects of rare earth and other elements used in magnesium alloys on primary cells and cell lines, *Acta Biomater.*, 2010, **6**, 1834.
61 Y. F. Ding, J. X. Lin, C. Wen, D. M. Zhang and Y. C. Li, Mechanical properties, *in vitro* corrosion and biocompatibility of newly developed biodegradable Mg–Zr–Sr–Ho alloys for biomedical applications, *Sci. Rep.*, 2016, **6**, 31990.
62 E. Mendive-Tapia and J. B. Staunton, Theory of Magnetic Ordering in the Heavy Rare Earths: *Ab Initio* Electronic Origin of Pair- and Four-Spin Interactions, *Phys. Rev. Lett.*, 2017, **118**, 197202.
63 K. P. Skokov and O. Gutfleisch, Heavy rare earth free, free rare earth and rare earth free magnets-Vision and reality, *Scr. Mater.*, 2018, **154**, 289.
64 S. B. Cheng, C. Berkdemir and A. W. Castleman Jr, Mimicking the magnetic properties of rare earth elements using superatoms, *Proc. Natl. Acad. Sci. U. S. A.*, 2015, **112**, 4941.
65 S. Gabani, K. Flachbart, K. Siemensmeyer and T. Mori, Magnetism and superconductivity of rare earth borides, *J. Alloys Compd.*, 2020, **821**, 153201.

66 Y. Hinatsu and Y. Doi, Magnetic interactions in new fluorite-related rare earth oxides $LnLn'_2RuO_7$ (Ln, Ln′ = rare earths), *J. Solid State Chem.*, 2016, **239**, 214.
67 P. L. Gao, Y. H. Xia, J. Gong and X. Ju, Structure and Magnetic Properties of $ErFe_xMn_{12-x}$ ($7.0 \leq x \leq 9.0$, Deltax = 0.2), *Nanomaterials*, 2022, **9**, 1586.
68 A. S. Patil, A. V. Patil, C. G. Dighavkar, V. A. Adole and U. J. Tupe, Synthesis techniques and applications of rare earth metal oxides semiconductors: a review, *Chem. Phys. Lett.*, 2022, **796**, 139555.
69 T. H. Wang, Z. K. Ma, Q. H. Zhu, L. J. Yang, B. S. Liu, Y. Zhao, C. Xu, B. Z. Zheng, F. Q. Hu, J. Z. Li, Q. F. Huang and Z. L. Song, Effect of aluminum on microstructure and magnetic properties of sintered Nd-Fe-B magnets processed by grain boundary diffusion of Tb-Al, *J. Rare Earths*, 2022, **4**, 017.
70 H. Nakamura, The current and future status of rare earth permanent magnets, *Scr. Mater.*, 2018, **154**, 273.
71 H. Wakayama and H. Yonekura, Use of block copolymer templates for chemical synthesis of $Nd_2Fe_{14}B$ nanocomposites with controlled magnetic properties, *Mater. Chem. Phys.*, 2019, **227**, 265.
72 J. J. Xu, K. Zhu, S. Gao and Y. L. Hou, Rare earth permanent magnetic nanostructures: chemical design and microstructure control to optimize magnetic properties, *Inorg. Chem. Front.*, 2021, **8**, 383.
73 Y. L. Hou, Z. C. Xu, S. Peng, C. Rong, J. P. Liu and S. Sun, A Facile Synthesis of $SmCo_5$ Magnets from Core/Shell Co/Sm_2O_3 Nanoparticles, *Adv. Mater.*, 2007, **19**, 3349.
74 Z. H. Ma, S. X. Yang, T. L. Zhang and C. B. Jiang, The chemical synthesis of $SmCo_5$ single-crystal particles with small size and high performance, *Chem. Eng. J.*, 2016, **304**, 993.
75 F. Lu, S. Xu and L. H. Wang, Pressure-induced magnetic transition in $Nd_2Fe_{14}B$ based on two-sublattice model, *Rare Met.*, 2019, **41**, 232.
76 P. K. Deheri, V. Swaminathan, S. D. Bhame, Z. W. Liu and R. V. Ramanujan, Sol-Gel Based Chemical Synthesis of $Nd_2Fe_{14}B$ Hard Magnetic Nanoparticles, *Chem. Mater.*, 2010, **22**, 6509.
77 C. Q. Chen, D. Kim and C. Choi, Influence of Ca amount on the synthesis of $Nd_2Fe_{14}B$ particles in reduction–diffusion process, *J. Magn. Magn. Mater.*, 2014, **355**, 180.
78 K. Zhu, J. J. Xu, X. B. Wang, W. Li, K. S. Tian and Y. L. Hou, Chemical synthesis and coercivity enhancement of $Nd_2Fe_{14}B$ nanostructures mediated by non-magnetic layer, *Nano Res.*, 2020, **13**, 1141.
79 A. Pal, A. Gabay and G. C. Hadjipanayis, Mechanochemical synthesis of $Nd_2Fe_{14}B$ alloy with high coercivity, *J. Alloys Compd.*, 2012, **543**, 31.
80 B. Z. Cui, L. Y. Zheng, W. F. Li, J. F. Liu and G. C. Hadjipanayis, Single-crystal and textured polycrystalline $Nd_2Fe_{14}B$ flakes with a submicron or nanosize thickness, *Acta Mater.*, 2012, **60**, 1721.
81 L. Q. Yu, C. Yang and Y. L. Hou, Controllable $Nd_2Fe_{14}B/\alpha$-Fe nanocomposites: chemical synthesis and magnetic properties, *Nanoscale*, 2014, **6**, 10638.
82 H. Parmar, T. Xiao, V. Chaudhary, Y. Zhong and R. V. Ramanujan, High energy product chemically synthesized exchange coupled $Nd_2Fe_{14}B/\alpha$-Fe magnetic powders, *Nanoscale*, 2017, **9**, 13956.
83 K. A. Gschneidner and V. K. Pecharsky, Rare Earths and Magnetic Refrigeration, *J. Rare Earths*, 2006, **24**, 641.
84 L. W. Li and M. Yan, Recent progresses in exploring the rare earth based intermetallic compounds for cryogenic magnetic refrigeration, *J. Alloys Compd.*, 2020, **823**, 153810.
85 L. W. Li and M. Yan, Recent progress in the magnetic and cryogenic magnetocaloric properties of RE_2TMTMO_6 double perovskite oxides, *J. Mater. Sci. Technol.*, 2022, **1**, 041.
86 L. H. Yin, J. Yang, P. Tong, X. Luo, C. B. Park, K. W. Shin, W. H. Song, J. M. Dai, K. H. Kim, X. B. Zhu and Y. P. Sun, Role of rare earth ions in the magnetic, magnetocaloric and magnetoelectric properties of $RCrO_3$ (R = Dy, Nd, Tb, Er) crystals, *J. Mater. Chem. C*, 2016, **4**, 11198.
87 L. H. Yin, J. Yang, X. C. Kan, W. H. Song, J. M. Dai and Y. P. Sun, Giant magnetocaloric effect and temperature induced magnetization jump in $GdCrO_3$ single crystal, *J. Appl. Phys.*, 2015, **117**, 133901.
88 Y. He, S. H. Guo, K. H. Chen, S. W. Li, L. B. Zhang and S. H. Yin, Sustainable green production: a review of recent development on rare earths extraction and separation using microreactors, *ACS Sustainable Chem. Eng.*, 2019, **7**, 17616.
89 P. Sarfo, T. Frasz, A. Das and C. Young, Hydrometallurgical Recovery and Process Optimization of Rare Earth Fluorides from Recycled Magnets, *Minerals*, 2020, **21**, 17616.
90 H. G. Danielmeyer, Efficiency and fluorescence quenching of stoichiometric rare earth laser materials, *J. Lumin.*, 1976, **12**, 179.
91 H. Kang, J. L. Peng, Z. Zhang and W. Zhou, Fluorescent strengthening effect of co-doped inert rare earth ions (La^{3+}, Gd^{3+}, Lu^{3+}) on white-light-emitting of Eu-Tb coordination polymers, *J. Lumin.*, 2022, **247**, 118904.
92 S. K. Gupta, K. Sudarshan and R. M. Kadam, Optical nanomaterials with focus on rare earth doped oxide: a review, *Mater. Today Commun.*, 2021, **27**, 112277.
93 C. Kränkel, D. T. Marzahl, F. Moglia, G. Huber and P. W. Metz, Out of the blue: semiconductor laser pumped visible rare-earth doped lasers, *Laser Photonics Rev.*, 2016, **10**, 548.
94 Z. F. Wang, W. W. Ye, X. R. Luo and Z. G. Wang, Fabrication of Superhydrophobic and Luminescent Rare Earth/Polymer complex Films, *Sci. Rep.*, 2016, **6**, 24682.
95 L. J. He, J. L. Meng, J. Feng, Z. X. Zhang, X. J. Liu and H. J. Zhang, Insight into the Characteristics of 4f-Related Electronic Transitions for Rare-Earth-Doped $KLuS_2$ Luminescent Materials through First-Principles Calculation, *J. Phys. Chem. C*, 2019, **124**, 932.
96 S. V. Eliseeva and J. C. G. Bünzli, Rare earths: jewels for functional materials of the future, *New J. Chem.*, 2011, **35**, 1165.
97 Q. S. Wang, J. J. Li, M. N. Zhang and X. Li, A luminescent Eu(III)-based metal–organic framework as a highly

effective sensor for cation and anion detections, *Sens. Actuators, B*, 2018, **258**, 358.

98 R. Shi, B. H. Zhu, M. X. Hu, H. F. Zhou, J. M. Fan, Z. Tao, F. Chang and S. Y. Yu, Graphene oxide induced multi-layered six-petal flower-shaped rare earth Tb^{3+} hybrid luminescent material: synthesis, characterization, luminescence and fluorescence anti-counterfeiting properties, *J. Mater. Chem. C*, 2020, **8**, 2336.

99 Y. Wang, L. H. Wang, S. Y. Bao, L. Xu, J. D. Zhang, Y. Y. Liang, L. S. Wang, X. J. Liang and W. D. Xiang, High-performance and heat-resistant Ce:YAG phosphor in glass for laser lighting, *J. Alloys Compd.*, 2022, **921**, 166083.

100 S. Mukherjee, N. Pathak, K. Ali, D. Das and D. Dutta, Tailoring defect structure and dopant composition and the generation of various color characteristics in Eu^{3+} and Tb^{3+} doped MgF_2 phosphors, *Phys. Chem. Chem. Phys.*, 2022, **24**, 10915.

101 K. C. Wang, B. J. Zhao and L. Gao, X-ray photoemission spectroscopy investigation of $CaTiO_3$:Eu for luminescence property: effect of Eu^{3+} ion, *Mater. Res. Bull.*, 2016, **78**, 31.

102 X. Pan, L. F. Mei, Y. H. Wang, T. Seto, Y. X. Zhuang, Q. F. Guo, M. Plyaskin, W. Xi, C. Li, Y. S. Guo and L. B. Liao, Activators lattice migration strategy customized for tunable luminescence of Ce^{3+} doped β-$Ca_3(PO_4)_2$, *Chem. Eng. J.*, 2022, **446**, 137271.

103 J. Zhao, D. J. Mei, W. K. Wang, Y. D. Wu and D. F. Xue, Recent advances in nonlinear optical rare earth structures, *J. Rare Earths*, 2021, **39**, 1455.

104 T. Justel, C. R. Ronda and H. Nikol, Rare earth phosphors: fundamentals and applications, *J. Alloys Compd.*, 1998, **275**, 669.

105 A. Escudero, A. I. Becerro, C. Carrillo-Carrión, N. O. Núñez, M. V. Zyuzin, M. Laguna, D. González-Mancebo, M. Ocaña and W. J. Parak, Rare earth based nanostructured materials: synthesis, functionalization, properties and bioimaging and biosensing applications, *Nanophotonics*, 2017, **6**, 881.

106 Z. Y. Wang, L. S. Huang, C. C. Zhang, M. Y. Chuai, X. H. Zhang and M. Z. Zhang, The optical properties of Ce-doped SnS quantum dots with fast nanosecond lifetime, *J. Alloys Compd.*, 2019, **799**, 425.

107 S. Silvi, M. Baroncini, M. La Rosa and A. Credi, Interfacing Luminescent Quantum Dots with Functional Molecules for Optical Sensing Applications, *Top. Curr. Chem.*, 2016, **374**, 65.

108 B. Yan, H. C. Wu, P. T. Ma, J. Y. Niu and J. P. Wang, Recent advances in rare earth co-doped luminescent tungsten oxygen complexes, *Inorg. Chem. Front.*, 2021, **8**, 4158.

109 W. C. Zhan, Y. Guo, X. Q. Gong, Y. L. Guo, Y. Q. Wang and G. Z. Lu, Current status and perspectives of rare earth catalytic materials and catalysis, *Chin. J. Catal.*, 2014, **35**, 1238.

110 Z. Q. Hou, W. B. Pei, X. Zhang, K. F. Zhang, Y. X. Liu, J. G. Deng, L. Jing and H. X. Dai, Rare earth oxides and their supported noble metals in application of environmental catalysis, *J. Rare Earths*, 2020, **38**, 819.

111 S. Zhang, S. E. Saji, Z. Yin, H. Zhang, Y. Du and C. H. Yan, Rare-Earth Incorporated Alloy Catalysts: Synthesis, Properties, and Applications, *Adv. Mater.*, 2021, **33**, e2005988.

112 X. C. Sun, K. Yuan and Y. W. Zhang, Advances and prospects of rare earth metal–organic frameworks in catalytic applications, *J. Rare Earths*, 2020, **38**, 801.

113 R. Burch, Knowledge and Know-How in Emission Control for Mobile Applications, *Catal. Rev.*, 2011, **46**, 271.

114 T. Fujita, H. Abe, T. Tanabe, Y. Ito, T. Tokunaga, S. Arai, Y. Yamamoto, A. Hirata and M. Chen, Earth-Abundant and Durable Nanoporous Catalyst for Exhaust-Gas Conversion, *Adv. Funct. Mater.*, 2016, **26**, 1609.

115 H. Tanaka, I. Tan, M. Uenishi, M. Taniguchi, M. Kimura, Y. Nishihata and J. i. Mizuki, $LaFePdO_3$ perovskite automotive catalyst having a self-regenerative function, *J. Alloys Compd.*, 2006, **408**, 1071.

116 Q. Hu, K. Cao, Y. Lang, R. Chen, S. Q. Chu, L. W. Jia, J. Yue and B. Shan, Improved NO-CO reactivity of highly dispersed Pt particles on CeO_2 nanorod catalysts prepared by atomic layer deposition, *Catal. Sci. Technol.*, 2019, **9**, 2664.

117 Y. W. Jiang, J. H. Gao, Q. Zhang, Z. Y. Liu, M. L. Fu, J. L. Wu, Y. Hu and D. Q. Ye, Enhanced oxygen vacancies to improve ethyl acetate oxidation over MnO_x-CeO_2 catalyst derived from MOF template, *Chem. Eng. J.*, 2019, **371**, 78.

118 Y. Y. Wang, D. H. Wu, P. Lv, B. L. He, X. Li, D. W. Ma and Y. Jia, Theoretical insights into the electroreduction of nitrate to ammonia on the graphene-based single-atom catalyst, *Nanoscale*, 2022, **14**(30), 10862.

119 C. X. Wang, W. Z. Xia, D. X. Yang, T. T. Zheng, Y. J. Rong, J. C. Du, B. X. Wu and Y. K. Zhao, Understanding ammonia and nitrous oxide formation in typical three-way catalysis during the catalyst warm-up period, *J. Hazard. Mater.*, 2022, **438**, 129553.

120 H. Liu, Ammonia synthesis catalyst 100 years: practice, enlightenment and challenge, *Chin. J. Catal.*, 2014, **35**, 1619.

121 J. Fuller, A. Fortunelli, W. A. Goddard and Q. An, Reaction mechanism and kinetics for ammonia synthesis on the Fe(211) reconstructed surface, *Phys. Chem. Chem. Phys.*, 2019, **21**, 11444.

122 J. Ji, X. Yan, G. Qian, C. Peng, X. Duan and X. Zhou, Morphology and location manipulation of Fe nanoparticles on carbon nanofibers as catalysts for ammonia decomposition to generate hydrogen, *Int. J. Hydrogen Energy*, 2017, **42**, 17466.

123 W. W. E. Takeshita T and R. S. Craig, Rare earth intermetallics as synthetic ammonia catalysts, *J. Catal.*, 1976, **44**, 236.

124 A. K. I. Niwa Y, The promoter effect of lanthana on MgO supported ruthenium catalysts for ammonia synthesis, *Res. Chem. Intermed.*, 1998, **24**, 593.

125 K. Okura, T. Okanishi, H. Muroyama, T. Matsui and K. Eguchi, Ammonia Decomposition over Nickel Catalysts Supported on Rare-Earth Oxides for the On-Site Generation of Hydrogen, *ChemCatChem*, 2016, **8**, 2988.

126 W. Li, S. Wang and J. P. Li, Effect of rare earth elements (La, Y, Pr) in multi-element composite perovskite oxide supports for ammonia synthesis, *J. Rare Earths*, 2021, **39**, 427.
127 J. Baltrusaitis, Sustainable Ammonia Production, *ACS Sustainable Chem. Eng.*, 2017, **5**, 9527.
128 S. Ghavam, M. Vahdati, I. A. G. Wilson and P. Styring, Sustainable Ammonia Production Processes, *Front. Energy Res.*, 2021, **9**, 580808.
129 A. Kovač, M. Paranos and D. Marciuš, Hydrogen in energy transition: a review, *Int. J. Hydrogen Energy*, 2021, **46**, 10016.
130 J. O. Abe, A. P. I. Popoola, E. Ajenifuja and O. M. Popoola, Hydrogen energy, economy and storage: review and recommendation, *Int. J. Hydrogen Energy*, 2019, **44**, 15072.
131 T. Y. Wei, K. L. Lim, Y. S. Tseng and S. L. I. Chan, A review on the characterization of hydrogen in hydrogen storage materials, *Renewable Sustainable Energy Rev.*, 2017, **79**, 1122.
132 A. Kumar, P. Muthukumar, P. Sharma and E. A. Kumar, Absorption based solid state hydrogen storage system: a review, *Sustain. Energy Technol. Assessments*, 2022, **52**, 102204.
133 M. Bououdina, D. Grant and G. Walker, Review on hydrogen absorbing materials-structure, microstructure, and thermodynamic properties, *Int. J. Hydrogen Energy*, 2006, **31**, 177.
134 L. Z. Ouyang, F. Liu, H. Wang, J. W. Liu, X. S. Yang, L. X. Sun and M. Zhu, Magnesium-based hydrogen storage compounds: a review, *J. Alloys Compd.*, 2020, **832**, 154865.
135 S. Kumar, M. Samolia and T. J. Dhilip Kumar, Hydrogen Storage in Sc and Li Decorated Metal–Inorganic Framework, *ACS Appl. Energy Mater.*, 2018, **1**, 1328.
136 T. Sadhasivam, H. T. Kim, S. Jung, S. H. Roh, J. H. Park and H. Y. Jung, Dimensional effects of nanostructured Mg/MgH_2 for hydrogen storage applications: a review, *Renewable Sustainable Energy Rev.*, 2017, **72**, 523.
137 H. Chaib, L. Mohammedi, L. Benmebrouk, A. Boukraa, B. Daoudi and A. Achouri, Effect of metal atom substitutions in Li based hydrides for hydrogen storage, *Int. J. Hydrogen Energy*, 2020, **45**, 28920.
138 Y. D. Chen, S. Yu, W. H. Zhao, S. F. Li and X. M. Duan, A potential material for hydrogen storage: a Li decorated graphitic-CN monolayer, *Phys. Chem. Chem. Phys.*, 2018, **20**, 13473.
139 C. Briki, P. de Rango, S. Belkhiria, M. H. Dhaou and A. Jemni, Measurements of expansion of $LaNi_5$ compacted powder during hydrogen absorption/desorption cycles and their influences on the reactor wall, *Int. J. Hydrogen Energy*, 2019, **44**, 13647.
140 W. Liu and K. F. Aguey-Zinsou, Low temperature synthesis of $LaNi_5$ nanoparticles for hydrogen storage, *Int. J. Hydrogen Energy*, 2016, **41**, 1679.
141 Y. Wu, H. G. Yu, Y. R. Guo, Y. X. Zhang, X. J. Jiang, B. X. Sun, K. Fu, J. Chen, Y. Qi, J. Zheng and X. G. Li, Promoting hydrogen absorption of liquid organic hydrogen carriers by solid metal hydrides, *J. Mater. Chem. A*, 2019, **7**, 16677.
142 H. Shi, G. L. Liu and X. H. Hu, Accelerating electrochemical hydrogen evolution kinetics in alkaline media using LaNi5 as a hydrogen reservoir, *Chem. Commun.*, 2022, **58**, 7289.
143 T. von Waldkirch and P. Zürcher, Surface segregation in $LaNi_5$ induced by oxygen, *Appl. Phys. Lett.*, 1978, **33**, 689.
144 K. Goto, T. Hirata, I. Yamamoto and W. Nakao, Suitability Evaluation of $LaNi_5$ as Hydrogen-Storage-Alloy Actuator by *In Situ* Displacement Measurement during Hydrogen Pressure Change, *Molecules*, 2019, **24**, 2420.
145 H. G. Yu, Y. Wu, S. P. Chen, Z. W. Xie, Y. M. Wu, N. Cheng, X. Yang, W. Lin, L. Xie, X. G. Li and J. Zheng, Pd-modified $LaNi_5$ nanoparticles for efficient hydrogen storage in a carbazole type liquid organic hydrogen carrier, *Appl. Catal., B*, 2022, **317**, 121720.
146 M. Melnichuk, D. J. Cuscueta and N. Silin, $LaNi_5$ hydride powder flowability as a function of activation and hydrogen content, *Int. J. Hydrogen Energy*, 2017, **42**, 15799.
147 Y. Ye, Y. Yue, J. F. Lu, J. Ding, W. L. Wang and J. Y. Yan, Enhanced hydrogen storage of a $LaNi_5$ based reactor by using phase change materials, *Renewable Energy*, 2021, **180**, 734.
148 J. M. Joubert, V. Paul-Boncour, F. Cuevas, J. Zhang and M. Latroche, $LaNi_5$ related AB_5 compounds: structure, properties and applications, *J. Alloys Compd.*, 2021, **862**, 158163.
149 H. Cao, P. Georgopanos, G. Capurso, C. Pistidda, F. Weigelt, A. L. Chaudhary, V. Filiz, J. C. Tseng, M. T. Wharmby, M. Dornheim, V. Abetz and T. Klassen, Air-stable metal hydride-polymer composites of $Mg(NH_2)_2$-LiH and TP, *Mater. Today Energy*, 2018, **10**, 98.
150 L. Schlapbach, A. Züttel, P. Gröning, O. Gröning and P. Aebi, Hydrogen for novel materials and devices, *Appl. Phys. A: Mater. Sci. Process.*, 2001, **72**, 245.
151 K. J. Jeon, H. R. Moon, A. M. Ruminski, B. Jiang, C. Kisielowski, R. Bardhan and J. J. Urban, Air-stable magnesium nanocomposites provide rapid and high-capacity hydrogen storage without using heavy-metal catalysts, *Nat. Mater.*, 2011, **10**, 286.
152 H. Liang, D. D. Chen, M. F. Chen, W. J. Li and R. Snyders, Study of the synthesis of PMMA-Mg nanocomposite for hydrogen storage application, *Int. J. Hydrogen Energy*, 2020, **45**, 4743.
153 R. Pedicini, B. Schiavo, P. Rispoli, A. Saccà, A. Carbone, I. Gatto and E. Passalacqua, Progress in polymeric material for hydrogen storage application in middle conditions, *Energy*, 2014, **64**, 607.
154 R. Pedicini, A. Saccà, A. Carbone and E. Passalacqua, Hydrogen storage based on polymeric material, *Int. J. Hydrogen Energy*, 2011, **36**, 9062.
155 G. R. d. Almeida Neto, C. A. Gonçalves Beatrice, D. R. Leiva and L. A. Pessan, Polymer-based composite containing nanostructured $LaNi_5$ for hydrogen storage: improved air stability and processability, *Int. J. Hydrogen Energy*, 2020, **45**, 14017.
156 K. C. Majhi and M. Yadav, Facile hydrothermal synthesis of rare earth phosphate for boosting hydrogen evolution reaction, *Int. J. Hydrogen Energy*, 2022, **47**, 14092.

157 S. Suwarno, M. V. Lototskyy and V. A. Yartys, Thermal desorption spectroscopy studies of hydrogen desorption from rare earth metal trihydrides REH_3 (RE = Dy, Ho, Er), *J. Alloys Compd.*, 2020, **842**, 155530.

158 J. J. Liu, K. Li, H. H. Cheng, K. Yan, Y. Wang, Y. Liu, H. M. Jin and Z. Zheng, New insights into the hydrogen storage performance degradation and Al functioning mechanism of $LaNi_5$-Al alloys, *Int. J. Hydrogen Energy*, 2017, **42**, 24904.

159 L. J. Y. Han J I, Hybriding kinetics of $LaNi_5$ and $LaNi_{4.7}Al_{0.3}$, *Int. J. Hydrogen Energy*, 1989, **14**, 181.

160 S. Todorova, B. Abrashev, V. Rangelova, L. Mihaylov, E. Vassileva, K. Petrov and T. Spassov, Hydrogen Gas Phase and Electrochemical Hydriding of $LaNi_{5-x}M_x$ (M = Sn, Co, Al) Alloys, *Materials*, 2020, **14**, 14.

161 Z. Łodziana, A. Dębski, G. Cios and A. Budziak, Ternary $LaNi_{4.75}M_{0.25}$ hydrogen storage alloys: surface segregation, hydrogen sorption and thermodynamic stability, *Int. J. Hydrogen Energy*, 2019, **44**, 1760.

162 F. F. Azenwi, H. W. Langmi and G. Sean McGrady, Hydrogenation of LiH/Al catalyzed with TiN, $TiMn_2$ and $LaNi_5$, *Int. J. Hydrogen Energy*, 2012, **37**, 10210.

163 X. Ma, X. Wei, H. Dong and Y. Liu, The relationship between discharge capacity of $LaNi_5$ type hydrogen storage alloys and formation enthalpy, *J. Alloys Compd.*, 2010, **490**, 548.

164 S. Nowak and M. Winter, Elemental analysis of lithium ion batteries, *J. Anal. At. Spectrom.*, 2017, **32**, 1833.

165 T. C. Ouyang, B. L. Liu, P. H. Xu, C. C. Wang and J. Ye, Electrochemical-thermal coupled modelling and multi-measure prevention strategy for Li-ion battery thermal runaway, *Int. J. Heat Mass Transfer*, 2022, **194**, 123082.

166 S. Sahoo, R. Kumar, E. Joanni, R. K. Singh and J. J. Shim, Advances in pseudocapacitive and battery-like electrode materials for high performance supercapacitors, *J. Mater. Chem. A*, 2022, **10**, 13190.

167 L. Z. Zhou, H. Yang, T. T. Han, Y. Z. Song, G. T. Yang and L. S. Li, Carbon-Based Modification Materials for Lithium-ion Battery Cathodes: Advances and Perspectives, *Front. Chem.*, 2022, **10**, 914930.

168 S. Zhang, W. T. Deng, R. Momen, S. Y. Yin, J. Chen, A. Massoudi, G. Zou, H. S. Hou, W. N. Deng and X. B. Ji, Element substitution of a spinel $LiMn_2O_4$ cathode, *J. Mater. Chem. A*, 2021, **9**, 21532.

169 Z. Wang, J. T. Zhang, F. H. Dong, P. D. Liu, Y. M. Zhu, P. Gao, X. X. Huang and G. W. Wen, Density functional theory guidance on rare earth doping-inhibition of lattice oxygen evolution in lithium-rich layered manganese oxide materials, *J. Alloys Compd.*, 2022, **899**, 163311.

170 J. Henao, O. Sotelo, M. Casales-Diaz and L. Martinez-Gomez, Hydrogen storage in a rare-earth perovskite-type oxide $La_{0.6}Sr_{0.4}Co_{0.2}Fe_{0.8}O_3$ for battery applications, *Rare Met.*, 2018, **37**, 1003.

171 L. Xue, Q. H. Zhang, X. H. Zhu, L. Gu, J. L. Yue, Q. Y. Xia, T. Xing, T. T. Chen, Y. Yao and H. Xia, 3D $LiCoO_2$ nanosheets assembled nanorod arrays *via* confined dissolution-recrystallization for advanced aqueous lithium-ion batteries, *Nano Energy*, 2019, **56**, 463.

172 Q. H. Zhou, H. H. Xu, l. Lu, W. H. Liu, Y. Liang, H. L. Li and T. Chen, Study on the decline mechanism of cathode material $LiCoO_2$ for Li-ion battery, *Vacuum*, 2020, **177**, 109313.

173 Q. Liu, X. Su, D. Lei, Y. Qin, J. G. Wen, F. M. Guo, Y. A. Wu, Y. C. Rong, R. H. Kou, X. H. Xiao, F. Aguesse, J. Bareño, Y. Ren, W. Q. Lu and Y. X. Li, Approaching the capacity limit of lithium cobalt oxide in lithium ion batteries *via* lanthanum and aluminium doping, *Nat. Energy*, 2018, **3**, 936.

174 R. Kataoka, N. Taguchi, T. Kojima, N. Takeichi and T. Kiyobayashi, Improving the oxygen redox stability of NaCl-type cation disordered Li_2MnO_3 in a composite structure of Li_2MnO_3 and spinel-type $LiMn_2O_4$, *J. Mater. Chem. A*, 2019, **7**, 5381.

175 J. Lu, C. Zhan, T. Wu, J. Wen, Y. Lei, A. J. Kropf, H. Wu, D. J. Miller, J. W. Elam, Y. K. Sun, X. Qiu and K. Amine, Effectively suppressing dissolution of manganese from spinel lithium manganate *via* a nanoscale surface-doping approach, *Nat. Commun.*, 2014, **5**, 5693.

176 P. Ram, A. Gören, S. Ferdov, M. M. Silva, R. Singhal, C. M. Costa, R. K. Sharma and S. Lanceros-Méndez, Improved performance of rare earth doped $LiMn_2O_4$ cathodes for lithium-ion battery applications, *New J. Chem.*, 2016, **40**, 6244.

177 R. Singhal, S. R. Das, M. S. Tomar, O. Ovideo, S. Nieto, R. E. Melgarejo and R. S. Katiyar, Synthesis and characterization of Nd doped $LiMn_2O_4$ cathode for Li-ion rechargeable batteries, *J. Power Sources*, 2007, **164**, 857.

178 L. Xia, K. H. Qiu, Y. Y. Gao, X. He and F. D. Zhou, High potential performance of Cerium-doped $LiNi_{0.5}Co_{0.2}Mn_{0.3}O_2$ cathode material for Li-ion battery, *J. Mater. Sci.*, 2015, **50**, 2914.

179 Y. W. Tian, X. X. Kang, L. Y. Liu, C. Q. Xu and T. Qu, Research on cathode material of Li-ion battery by yttrium doping, *J. Rare Earths*, 2008, **26**, 279.

180 I. Rabani, Y. J. Park, J. W. Lee, M. S. Tahir, A. Kumar and Y. S. Seo, Ultra-thin flexible paper of BNNT–CNF/ZnO ternary nanostructure for enhanced solid-state supercapacitor and piezoelectric response, *J. Mater. Chem. A*, 2022, **10**(29), 15580.

181 K. F. Chen, G. Li and D. F. Xue, Architecture engineering of supercapacitor electrode materials, *Funct. Mater. Lett.*, 2016, **9**, 1640001.

182 D. C. Grahame, Properties of the electrical double layer at a mercury surface. I. Methods of measurement and interpretation of results, *J. Am. Chem. Soc.*, 1941, **63**, 1207.

183 B. E. Conway, Transition from "supercapacitor" to "battery" behavior in electrochemical energy storage, *J. Electrochem. Soc.*, 1991, **138**, 1539.

184 V. Augustyn, P. Simon and B. Dunn, Pseudocapacitive oxide materials for high-rate electrochemical energy storage, *Energy Environ. Sci.*, 2014, **7**(5), 1597.

185 Y. Zhou, H. L. Qi, J. Y. Yang, Z. Bo, F. Huang, M. S. Islam, X. Y. Lu, L. M. Dai, R. Amal, C. H. Wang and Z. J. Han,

Two-birds-one-stone: multifunctional supercapacitors beyond traditional energy storage, *Energy Environ. Sci.*, 2021, **14**, 1854.

186 G. Z. Chen, Supercapacitor and supercapattery as emerging electrochemical energy stores, *Int. Mater. Rev.*, 2016, **62**, 173.

187 A. Laheäär, P. Przygocki, Q. Abbas and F. Béguin, Appropriate methods for evaluating the efficiency and capacitive behavior of different types of supercapacitors, *Electrochem. Commun.*, 2015, **60**, 21.

188 P. Cai, K. Y. Zou, X. L. Deng, B. W. Wang, M. Zheng, L. H. Li, H. S. Hou, G. Q. Zou and X. B. Ji, Comprehensive Understanding of Sodium-Ion Capacitors: Definition, Mechanisms, Configurations, Materials, Key Technologies, and Future Developments, *Adv. Energy Mater.*, 2021, **11**, 2003804.

189 T. Schoetz, L. W. Gordon, S. Ivanov, A. Bund, D. Mandler and R. J. Messinger, Disentangling faradaic, pseudocapacitive, and capacitive charge storage: a tutorial for the characterization of batteries, supercapacitors, and hybrid systems, *Electrochim. Acta*, 2022, **412**, 140072.

190 B. E. Conway and E. Gileadi, Kinetic theory of pseudo-capacitance and electrode reactions at appreciable surface coverage, *Trans. Faraday Soc.*, 1962, **58**, 2494.

191 H. L. Yang, H. H. Xu, L. B. Wang, L. Zhang, Y. L. Huang and X. H. Hu, Microwave-Assisted Rapid Synthesis of Self-Assembled T-Nb_2O_5 Nanowires for High-Energy Hybrid Supercapacitors, *Chemistry*, 2017, **23**, 4203.

192 X. Q. Bin, Y. P. Tian, Y. Y. Luo, M. H. Sheng, Y. J. Luo, M. M. Ju and W. X. Que, High-performance flexible and free-standing N-doped Ti_3C_2T/MoO films as electrodes for supercapacitors, *Electrochim. Acta*, 2021, **389**, 38774.

193 R. Ma, Z. T. Chen, D. N. Zhao, X. J. Zhang, J. T. Zhuo, Y. J. Yin, X. F. Wang, G. W. Yang and F. Yi, $Ti_3C_2T_x$ MXene for electrode materials of supercapacitors, *J. Mater. Chem. A*, 2021, **9**, 11501.

194 M. M. Hu, H. Zhang, T. Hu, B. B. Fan, X. H. Wang and Z. J. Li, Emerging 2D MXenes for supercapacitors: status, challenges and prospects, *Chem. Soc. Rev.*, 2020, **49**, 6666.

195 H. Y. Zhao, J. L. Xia, D. D. Yin, M. Luo, C. H. Yan and Y. P. Du, Rare earth incorporated electrode materials for advanced energy storage, *Coord. Chem. Rev.*, 2019, **390**, 32.

196 D. B. Bailmare, P. Tripathi, A. D. Deshmukh and B. K. Gupta, Designing of two dimensional lanthanum cobalt hydroxide engineered high performance supercapacitor for longer stability under redox active electrolyte, *Sci. Rep.*, 2022, **12**, 3084.

197 K. M. Thulasi, S. T. Manikkoth, A. Paravannoor, S. Palantavida, M. Bhagiyalakshmi and B. K. Vijayan, Ceria deposited titania nanotubes for high performance supercapacitors, *J. Phys. Chem. Solids*, 2019, **135**, 109111.

198 A. K. Das, U. N. Pan, V. Sharma, N. H. Kim and J. H. Lee, Nanostructured CeO_2/NiV–LDH composite for energy storage in asymmetric supercapacitor and as methanol oxidation electrocatalyst, *Chem. Eng. J.*, 2021, **417**, 128019.

199 S. F. Liang, H. Y. Wang, Y. Li, H. Z. Qin, Z. Y. Luo, B. Huang, X. Zhao, C. L. Zhao and L. Y. Chen, Rare-earth based nanomaterials and their composites as electrode materials for high performance supercapacitors: a review, *Sustainable Energy Fuels*, 2020, **4**, 3825.

200 J. D. Wang, X. Xiao, Y. Liu, K. M. Pan, H. Pang and S. Z. Wei, The application of CeO_2-based materials in electrocatalysis, *J. Mater. Chem. A*, 2019, **7**, 17675.

201 C. W. Sun, H. Li and L. Q. Chen, Nanostructured ceria-based materials: synthesis, properties, and applications, *Energy Environ. Sci.*, 2012, **5**, 8475.

202 N. Maheswari and G. Muralidharan, Supercapacitor Behavior of Cerium Oxide Nanoparticles in Neutral Aqueous Electrolytes, *Energy Fuels*, 2015, **29**, 8246.

203 L. Wang, Y. H. Li, M. Shi, W. L. Ma and H. T. Cui, Synthesis of CeO_2 nanocrystals with controlled size and shape and their influence on electrochemical performance, *J. Sol-Gel Sci. Technol.*, 2017, **83**(2), 308.

204 X. D. Hao, S. Zhang, Y. Xu, L. Y. Tang, K. Inoue, M. Saito, S. F. Ma, C. L. Chen, B. S. Xu, T. Adschiri and Y. Ikuhara, Surfactant-mediated morphology evolution and self-assembly of cerium oxide nanocrystals for catalytic and supercapacitor applications, *Nanoscale*, 2021, **13**, 10393.

205 C. X. Cheng, F. Chen, H. Y. Yi and G. S. Lai, CeO_2 mesoporous microspheres for high performance supercapacitors and lithium-ion batteries, *J. Energy Storage*, 2021, **35**, 102305.

206 A. J. Khan, M. Hanif, M. S. Javed, S. Hussain, W. J. Zhong, M. Saleem and Z. W. Liu, Energy storage properties of hydrothermally processed, nanostructured, porous CeO_2 nanoparticles, *J. Electroanal. Chem.*, 2020, **865**, 114158.

207 N. Maheswari and G. Muralidharan, Hexagonal CeO_2 nanostructures: an efficient electrode material for supercapacitors, *Dalton Trans.*, 2016, **45**, 14352.

208 K. Prasanna, P. Santhoshkumar, Y. N. Jo, I. N. Sivagami, S. H. Kang, Y. C. Joe and C. W. Lee, Highly porous CeO_2 nanostructures prepared *via* combustion synthesis for supercapacitor applications, *Appl. Surf. Sci.*, 2018, **449**, 454.

209 M. Kumar, J. H. Yun, V. Bhatt, B. Singh, J. Kim, J. S. Kim, B. S. Kim and C. Y. Lee, Role of Ce^{3+} valence state and surface oxygen vacancies on enhanced electrochemical performance of single step solvothermally synthesized CeO_2 nanoparticles, *Electrochim. Acta*, 2018, **284**, 709.

210 G. Nabi, W. Ali, A. Majid, T. Alharbi, S. Saeed and M. A. Albedah, Controlled growth of Bi-functional La doped CeO_2 nanorods for photocatalytic H_2 production and supercapacitor applications, *Int. J. Hydrogen Energy*, 2022, **47**, 15480.

211 T. Kar, M. Casales-Diaz, J. J. Ramos-Hernandez, O. Sotelo-Mazon, J. Henao, S. Valdez Rodriguez, S. Godavarthi, S. Liu, Y. Yamauchi and M. K. Kesarla, CeO_{2-x} quantum dots decorated nitrogen-doped hollow porous carbon for supercapacitors, *J. Colloid Interface Sci.*, 2022, **622**, 147.

212 Y. Luo, T. Y. Yang, Q. Zhao and M. Z. Zhang, CeO_2/CNTs hybrid with high performance as electrode materials for supercapacitor, *J. Alloys Compd.*, 2017, **729**, 64.

213 W. J. Wu, W. T. Qi, Y. F. Zhao, X. Tang, Y. F. Qiu, D. W. Su, H. B. Fan and G. X. Wang, Hollow CeO_2 spheres conformally coated with graphitic carbon for high-

performance supercapacitor electrodes, *Appl. Surf. Sci.*, 2019, **463**, 244.

214 B. Ramulu, G. Nagaraju, S. C. Sekhar and J. S. Yu, Highly porous CNTs knotted cerium oxide hollow tubes with exalted energy storage performance for hybrid supercapacitors, *J. Alloys Compd.*, 2020, **819**, 152942.

215 A. Jeyaranjan, T. S. Sakthivel, C. J. Neal and S. Seal, Scalable ternary hierarchical microspheres composed of PANI/rGO/CeO_2 for high performance supercapacitor applications, *Carbon*, 2019, **151**, 192.

216 A. J. Xie, F. Tao, T. Li, L. Wang, S. J. Chen, S. P. Luo and C. Yao, Graphene-cerium oxide/porous polyaniline composite as a novel electrode material for supercapacitor, *Electrochim. Acta*, 2018, **261**, 314.

217 M. Z. Zhong, M. Zhang and X. F. Li, Carbon nanomaterials and their composites for supercapacitors, *Carbon Energy*, 2022, **1**, 36.

218 M. Nallappan and M. Gopalan, Fabrication of CeO_2/PANI composites for high energy density supercapacitors, *Mater. Res. Bull.*, 2018, **106**, 357.

219 D. Biswas, A. S. Das, R. Mondal, A. Banerjee, A. Dutta, S. Kabi, D. Roy and L. S. Singh, Structural properties and electrical conductivity mechanisms of semiconducting quaternary nanocomposites: effect of two transition metal oxides, *J. Phys. Chem. Solids*, 2020, **144**, 109505.

220 K. Chen, X. M. Zhang, X. F. Yang, M. G. Jiao, Z. Zhou, M. H. Zhang, D. H. Wang and X. H. Bu, Electronic structure of heterojunction MoO_2/g-C_3N_4 catalyst for oxidative desulfurization, *Appl. Catal., B*, 2018, **238**, 263.

221 Z. Jiang, W. Wan, H. Li, S. Yuan, H. Zhao and P. K. Wong, A Hierarchical Z-Scheme alpha-Fe_2O_3/g-C_3N_4 Hybrid for Enhanced Photocatalytic CO_2 Reduction, *Adv. Mater.*, 2018, **30**(10), 1706108.

222 J. Y. Tang, R. T. Guo, W. G. Zhou, C. Y. Huang and W. G. Pan, Ball-flower like NiO/g-C_3N_4 heterojunction for efficient visible light photocatalytic CO_2 reduction, *Appl. Catal., B*, 2018, **237**, 802.

223 L. Zhang, S. S. Chai, W. B. Zhang, S. B. Guo, X. W. Han, Y. W. Guo, X. Bao and X. J. Ma, Cobalt boride on clay minerals for electrochemical capacitance, *Appl. Clay Sci.*, 2022, **218**, 802.

224 A. A. Yadav, A. C. Lokhande, J. H. Kim and C. D. Lokhande, Supercapacitive activities of porous La_2O_3 symmetric flexible solid-state device by hydrothermal method, *Int. J. Hydrogen Energy*, 2016, **41**, 18311.

225 A. A. Yadav, A. C. Lokhande and C. D. Lokhande, A simple chemical route for synthesis of microrods-like La_2O_3 thin films, *Mater. Lett.*, 2015, **160**, 500.

226 G. S. Gund, D. P. Dubal, S. B. Jambure, S. S. Shinde and C. D. Lokhande, Temperature influence on morphological progress of $Ni(OH)_2$ thin films and its subsequent effect on electrochemical supercapacitive properties, *J. Mater. Chem. A*, 2013, **1**, 4793.

227 K. L. Fang, J. Z. Chen, X. Y. Zhou, C. T. Mei, Q. H. Tian, J. L. Xu and C. P. Wong, Decorating biomass-derived porous carbon with Fe_2O_3 ultrathin film for high-performance supercapacitors, *Electrochim. Acta*, 2018, **261**, 198.

228 A. A. Yadav, A. C. Lokhande, R. B. Pujari, J. H. Kim and C. D. Lokhande, The synthesis of multifunctional porous honey comb-like La_2O_3 thin film for supercapacitor and gas sensor applications, *J. Colloid Interface Sci.*, 2016, **484**, 51.

229 J. Wang, J. w. Zhang, S. Liu, X. y. Pei, Y. Li and C. w. Wang, The accurate control of the La_2O_3 hierarchical structure of the flower-like microspheres accompanied with vertical-standing nanopetals and the electrowetting responses with low voltage actuation, *Ceram. Int.*, 2020, **46**, 11232.

230 A. A. Yadav, A. C. Lokhande, J. H. Kim and C. D. Lokhande, High electrochemical performance asymmetric supercapacitor based on La_2O_3//Co_3O_4 electrodes, *J. Ind. Eng. Chem.*, 2017, **56**, 90.

231 J. Sun, A. Iakunkov, A. T. Rebrikova and A. V. Talyzin, Exactly matched pore size for the intercalation of electrolyte ions determined using the tunable swelling of graphite oxide in supercapacitor electrodes, *Nanoscale*, 2018, **10**, 21386.

232 J. X. Zhang, Z. Z. Zhang, Y. T. Jiao, H. X. Yang, Y. Q. Li, J. Zhang and P. Gao, The graphene/lanthanum oxide nanocomposites as electrode materials of supercapacitors, *J. Power Sources*, 2019, **419**, 99.

233 S. Karthikeyan, M. Selvapandiyan and A. Sankar, Electrochemical performance of reduced graphene oxide (rGO) decorated lanthanum oxide (La_2O_3) composite nanostructure as asymmetric supercapacitors, *Inorg. Chem. Commun.*, 2022, **139**, 109331.

234 M. Miah, S. Bhattacharya, D. Dinda and S. K. Saha, Temperature dependent supercapacitive performance in La_2O_3 nano sheet decorated reduce graphene oxide, *Electrochim. Acta*, 2018, **260**, 449.

235 A. J. Webb, D. Bloor, M. Szablewski and D. Atkinson, Temperature dependence of electrical transport in a pressure-sensitive nanocomposite, *ACS Appl. Mater. Interfaces*, 2014, **6**, 12573.

236 B. G. Trasatti S, Ruthenium dioxide: a new interesting electrode material. Solid state structure and electrochemical behaviour, *J. Electroanal. Chem. Interfacial Electrochem.*, 1971, **29**, A1.

237 R. Liu, A. Zhou, X. R. Zhang, J. B. Mu, H. W. Che, Y. M. Wang, T. T. Wang, Z. X. Zhang and Z. K. Kou, Fundamentals, advances and challenges of transition metal compounds-based supercapacitors, *Chem. Eng. J.*, 2021, **412**, 128611.

238 C. X. Sun, W. X. Pan, D. Y. Zheng, R. B. Yao, Y. H. Zheng, J. H. Zhu and D. W. Jia, Low-Cost MnO_2 Nanoflowers and La_2O_3 Nanospheres as Efficient Electrodes for Asymmetric Supercapacitors, *Energy Fuels*, 2020, **34**, 14882.

239 H. Y. Duan, M. Shi, M. F. Zhang, G. Y. Feng, S. L. Liu and C. Y. Chen, Lanthanum Oxide Nickel Hydroxide Composite Triangle Nanosheets for Energy Density Asymmetric Supercapacitors, *Front. Chem.*, 2021, **9**, 783942.

240 Y. Li, B. Guan, A. Maclennan, Y. F. Hu, D. D. Li, J. Zhao, Y. Q. Wang and H. H. Zhang, Porous waxberry-like MnO_2/

La_2O_3 microspheres for high performance asymmetric supercapacitor, *Electrochim. Acta*, 2017, **241**, 395.

241 M. Majumder, R. B. Choudhary, A. K. Thakur, C. S. Rout and G. Gupta, Rare earth metal oxide (RE_2O_3; RE = Nd, Gd, and Yb) incorporated polyindole composites: gravimetric and volumetric capacitive performance for supercapacitor applications, *New J. Chem.*, 2018, **42**, 5295.

242 H. Mohammad Shiri and A. Ehsani, Electrosynthesis of neodymium oxide nanorods and its nanocomposite with conjugated conductive polymer as a hybrid electrode material for highly capacitive pseudocapacitors, *J. Colloid Interface Sci.*, 2017, **495**, 102.

243 P. Liu, Y. J. Wang, X. Wang, C. Yang and Y. F. Yi, Polypyrrole-coated samarium oxide nanobelts: fabrication, characterization, and application in supercapacitors, *J. Nanopart. Res.*, 2012, **14**, 1232.

244 H. Mohammad Shiri, A. Ehsani and M. Jalali Khales, Electrochemical synthesis of Sm_2O_3 nanoparticles: application in conductive polymer composite films for supercapacitors, *J. Colloid Interface Sci.*, 2017, **505**, 940.

245 M. Mazloum-Ardakani, F. Sabaghian, H. Naderi, A. Ebadi and H. Mohammadian-Sarcheshmeh, Electrochemical and theoretical study of novel functional porous graphene aerogel-supported Sm_2O_3 nanoparticles for supercapacitor applications, *J. Solid State Electrochem.*, 2020, **24**, 571.

246 H. Mohammad Shiri and A. Ehsani, A simple and innovative route to electrosynthesis of Eu_2O_3 nanoparticles and its nanocomposite with p-type conductive polymer: characterisation and electrochemical properties, *J. Colloid Interface Sci.*, 2016, **473**, 126.

247 H. M. Shiri and A. Ehsani, Pulse electrosynthesis of novel wormlike gadolinium oxide nanostructure and its nanocomposite with conjugated electroactive polymer as a hybrid and high efficient electrode material for energy storage device, *J. Colloid Interface Sci.*, 2016, **484**, 70.

248 V. Thangadurai, R. A. Huggins and W. Weppner, Mixed ionic-electronic conductivity in phases in the praseodymium oxide system, *J. Solid State Electrochem.*, 2001, **5**, 531.

249 X. Wang, C. Yang, T. M. Wang and P. Liu, Praseodymium oxide/polypyrrole nanocomposites for electrochemical energy storage, *Electrochim. Acta*, 2011, **58**, 193.

250 K. T. Kubra, A. Javaid, B. Patil, R. Sharif, A. Salman, S. Shahzadi, S. Siddique and S. Ghani, Synthesis and characterization of novel Pr_6O_{11}/Mn_3O_4 nanocomposites for electrochemical supercapacitors, *Ceram. Int.*, 2019, **45**, 6819.

251 N. Chen, A. Younis, S. H. Huang, D. W. Chu and S. Li, Advanced three-dimensional hierarchical Pr_6O_{11}@Ni-Co oxides-based core–shell electrodes for supercapacitance application, *J. Alloys Compd.*, 2019, **783**, 772.

252 A. Paravannoor, C. A. Augustine and N. Ponpandian, Rare earth nanostructures based on PrO_x/CNT composites as potential electrodes for an asymmetric pseudocapacitor cell, *J. Rare Earths*, 2020, **38**, 625.